Electron Transfer Model for the Electric Field Effect on Quantum Yield of Charge Separation in Bacterial Photosynthetic Reaction Centers

Shigenori Tanaka† and R. A. Marcus*

Arthur Amos Noyes Laboratory of Chemical Physics, California Institute of Technology, Pasadena, California 91125

Received: October 22, 1996; In Final Form: April 11, 1997[®]

The effect of an electric field on a photoinduced charge separation process is treated theoretically. The system considered is a reaction center (RC) of photosynthetic bacteria, involving an electron transfer (ET) from the electronically excited singlet state of the bacteriochlorophyll dimer (P) to the bacteriopheophytin (H) and quinone (Q). In contrast to formulations which focus only on the *forward* steps and do not explain the major effect on the quantum yield of P^+Q^- or, in Q-depleted samples, of P^+H^- , the present study includes the effect on the back reactions, an effect which we find to be large. The low-frequency medium and high-frequency intramolecular vibrational modes are included in the calculation of the various ET rates. Recent experimental results on the ET energetics, including the estimated effect of static heterogeneity in RCs, are incorporated. The rate equations for the population densities of distinct states are solved for both oriented and randomly oriented (isotropic) RC samples, and the results are compared with experimental data for the field-induced reduction of the quantum yield of formation of charge-separated state P^+Q^- . A simple (quasi-equilibrium) model calculation illustrates the essential features of this analysis of the electric field effect and compares reasonably well with these numerical results of the more detailed model. The question of the electric field effect on the fluorescence quantum yield is also addressed, and a suggestion is made for consistency with the data on the formation of P^+Q^- .

1. Introduction

The reaction center (RC) of purple photosynthetic bacteria provides an interesting system for studying a high-efficiency long-range electron transfer (ET) in an organized molecular assembly. In the RC complexes, the photoexcitation of a bacteriochlorophyll dimer (P) initiates a series of ET reactions along one side (L) of two symmetrically positioned pigment chains (Figure 1): The singlet excited dimer (¹P*) transfers an electron to a bacteriopheophytin (H) to form a P+H- radical pair. Subsequently, the electron moves to a quinone (Q) in a few hundred picoseconds, forming P⁺Q⁻ with a quantum yield of nearly unity, and this O⁻ later transfers its electron to a second quinone. One of the longstanding puzzles in these ET processes, and still unsettled, is the role of the accessory bacteriochlorophyll monomer (B) which is located between P and H. Two sites, later realized to be B and H, were postulated in an early study¹ to explain a contrast between the rate of the fast initial forward step and the weak interaction of P⁺ and H⁻ that was inferred from magnetic field studies.

According to the X-ray diffraction studies of the RCs from *Rhodopseudomonas (Rps.) viridis*^{2–4} and *Rhodobacter (Rb.) sphaeroides*,^{5–7} the center-to-center distance between P and H is approximately 17 Å (edge-to-edge distance is *ca.* 10 Å). The ultrafast ET between them, which occurs in a few picoseconds, then suggests that the electron is unlikely to be transferred directly and that B should play an indispensable role in this ET reaction. Extensive experimental efforts with time-resolved spectroscopic techniques have been devoted^{8–17} to elucidating this issue. At least two alternative models have been proposed for the role of B:^{1,18–21} In the two-step or sequential model, which is presently favored, the free energy of P+B-H is close

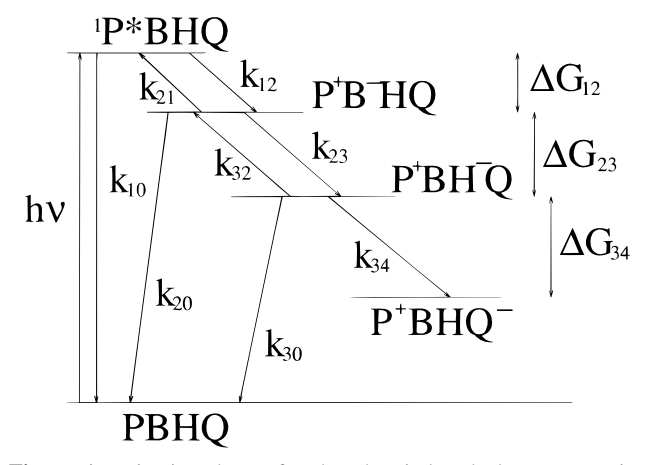


Figure 1. Kinetic scheme for the photoinduced charge-separation process in bacterial photosynthetic reaction centers used in the present analysis. P, $^1P^*$, B, H, and Q refer to the bacteriochlorophyll dimer, its singlet excited state, a bacteriochlorophyll monomer, a bacteriopheophytin, and a quinone, respectively. The k's and ΔG 's denote the rate constants and the free energy gaps.

to or lower than that of ¹P*BH, and P⁺B⁻H is supposed to be an actual intermediate, which then undergoes a subsequent ET from B to H. On the other hand, in the one-step or superexchange model, it is assumed that the radical pair state P⁺B⁻H has a free energy which lies well above that of ¹P*BH and is not formed as a distinct intermediate but instead serves as a virtual state which quantum-mechanically couples the ¹P*BH and P⁺BH⁻ states. In the experimental investigations, modified or mutant RCs have been used¹⁵⁻¹⁷ as well as wild-type and Q-depleted RCs to explore²¹ the kinetic consequences of the modification of free energy gaps between the pertinent states.

A further approach to studying experimentally the energetics associated with the ET reactions in RCs is to modify the kinetics by means of an externally applied electric field.²²⁻³³ For RC

^{*} Corresponding author.

[†] Permanent address: Toshiba Advanced Research Laboratory, 1 Komukai Toshiba-cho, Saiwai-ku, Kawasaki 210, Japan.

[⊗] Abstract published in *Advance ACS Abstracts*, June 1, 1997.

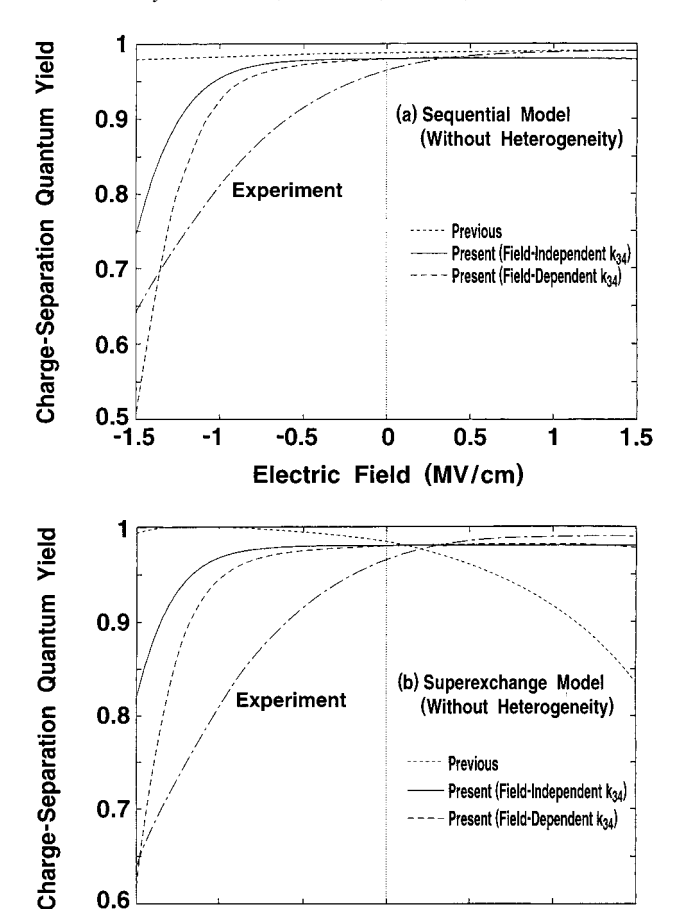


Figure 2. Simplified calculation for the electric field (F_{ext}) dependence of the charge-separation quantum yield Y_0 for the oriented RC sample at 295 K on the basis of (a) sequential and (b) superexchange ET models. Dotted curve: results obtained by eq 1.1, where $k_{\rm et} = k_{12}$ (a) and $k_{\rm et} = k_{13}$ (b) (cf. eqs A.15 and A.14). Solid curve: simplified approach, i.e., eq 2.8 (a) and eq A.16 (b), where k_{34} is fixed. Dashed curve: simplified approach, where an electric field dependence of k_{34} (cf. Figure 3b) is incorporated. The rate constants and the free energy gaps used in the calculations have been obtained according to the model given in section 2 (cf. Tables 1-3), and any effect of static heterogeneity12,15,35 for the free energy gaps is neglected here. Chain curve denotes the (fitted) experimental results.22

0

Electric Field (MV/cm)

0.5

-0.5

Present (Field-Dependent k34)

1.5

0.7

0.6

.5

samples oriented²² and randomly oriented²⁴⁻²⁶ with respect to the applied field, the quantum yields of the charge-separated states, P⁺H⁻ (in Q-depleted samples) and P⁺Q⁻, have proven to be reducible by 10-20% with an electric field of 1 MV/cm. This effect is interesting both from the viewpoint of understanding the ET energetics in RCs and for possible implications for the design of various energy conversion and switching devices.

Quantitative theoretical models to account for the experimental results on electric field effects have not yet been successful to date. It has been reasonably suggested34 that this field-induced quantum yield effect (QYE) arises from the change in the free energies of radical pair states due to their dipoles interacting with the electric field. However, if it is assumed that the charge-separation quantum yield is determined by the competition between the initial forward ET rate constant k_{et} and the decay rate constant k_{10} (which is the sum of radiative and nonradiative internal conversion rate constants, k_r and k_{nr}) of ${}^{1}P^{*}$, an extraordinarily strong dependence of k_{et} on the electric field would be required^{24,25,34} to explain the experimental QYE. The reason for this requirement is that $k_{\rm et}$ is larger than the k_{10} in Figure 1 by about 2 orders of magnitude. This difficulty is explicitly exhibited in Figure 2, which shows the electric field dependence of charge-separation quantum yield Y_Q for the oriented RC sample²² at 295 K. In the earlier models, ^{24,25,34} Yo is evaluated from (e.g., eq 2 in ref 25, eq IV.11 in ref 34, and a similar expression in ref 24)

$$Y_{\rm Q} = \frac{k_{\rm et}}{k_{10} + k_{\rm et}} \tag{1.1}$$

in both the sequential and superexchange ET models, where the rate constants have been calculated using the procedure given in section 2.

The purpose of the present paper is to explore an explanation for the effect of the electric field on the charge-separation quantum yield in photosynthetic RCs which focuses initially on a substantial effect on the back rate constants. For the sake of simplicity, mainly the sequential model for the primary ET is considered, since a similar explanation applies to the superexchange model. We use some current experimental estimates^{17,21} of the free energy gaps, reorganization energies, and other kinetic parameters for the ET reactions in RCs. According to a recent analysis^{17,21} of the energetics, the sequential ET channel dominates over the superexchange channel for the ${}^{1}P^{*}BH \rightarrow P^{+}BH^{-}$ reaction rate in wild-type RCs at room temperature, and a superexchange ET is important at low temperatures or in mutant RCs.21 An additional experimental suggestion in favor of the sequential model has been obtained in a study of the electric field effect on the initial step in oriented systems.²³ It has also been noted³⁶ recently that the sequential ET dominates at room temperature and that the sequential and superexchange ET mechanisms should not coexist as two parallel channels.

It will be seen through explicit calculations how an improved account of the experimental charge-separation QYE can be provided within the framework of the usual sequential ET model in a way consistent with other experimental facts on energetics and rates. Also, it is shown that a steady or quasi-equilibrium state realized in the primary ET processes, ${}^{1}P*BH \rightleftharpoons P^{+}B^{-}H$ \Rightarrow P⁺BH⁻, on the time scale of 10-100 ps after the photoexcitation, is important for understanding this aspect of the electric field effect on the quantum yields. Thereby, the back ET reactions play a significant role, in contrast with previous models based only on eq 1.1. Also given, and tested by comparison with the full numerical solution for oriented samples, is a simple approximate analytical expression for the quantum yields obtained by considering the temporal hierarchy among the reactions involved. We then consider the full calculation for the electric field effect on the fluorescence quantum vield to see whether the explanation for the charge-separation QYE also explains the effect on the fluorescence quantum yield, and if not, what other effect could plausibly be added to understand both sets of data consistently.

The paper is organized as follows: In section 2, the kinetic model used in the present analysis is described. Before giving a full treatment of the kinetic equations, a simplified approach based on the idea of a quasi-equilibrium state is considered first. It provides insight into the full calculation. In section 3 the calculated results are given for the time evolution of the population densities of the distinct states as a function of electric field. The electric field dependence of charge-separation quantum yield in RCs, for both oriented and randomly oriented samples with respect to the applied field, is then evaluated and compared with the experimental results in sections 3.1 and 3.2. The electric field effect on the fluorescence quantum yield in RCs is addressed in section 3.3. Also discussed in section 3 are the physical implications of the calculated results. A concluding summary is given in section 4. The influence on

TABLE 1: Rate Constants k_{ij} and Free Energy Gaps ΔG_{ij} at Zero External Electric Field Used in the Calculations

(i,j)	$1/k_{ij}$ (ps)	ref (k _{ij})	$\Delta G_{ij} (\mathrm{cm}^{-1})$	$\operatorname{ref}\left(\Delta G_{ij}\right)$
(1,0)	190 ^a	37	-11200	25
(2,0)	500	17	-10750^{d}	
(3,0)	10000^{b}	21	-9200^{e}	
(1,2)	2.3^{c}	17	-450^{f}	17
(2,3)	0.9^{c}	17	-1550^{g}	
(1,3)			-2000^{h}	39
(3,4)	200	17	-5200	42

^a Combined decay rate of ¹P*BH to PBH in all radiative and nonradiative channels^{37,38} except the charge-separation channel. ^b Overall recombination rate of P*BH⁻. ^c Value at T=295 K. ^d Calculated from ΔG_{10} and ΔG_{12} . ^e Not required for the present calculations. ^f Estimated¹⁷ from subpicosecond spectroscopy at room temperature for the modified RCs from *Rb. sphaeroides* in which bacteriopheophytins are replaced by pheophytins. This value is consistent with an estimate,²¹ –480 ± 180 cm⁻¹, derived from a kinetic analysis of the primary ET rates using experimental data for native and mutant RCs at room temperature. ^g Calculated from ΔG_{12} and ΔG_{13} ($\equiv \Delta G_{12} + \Delta G_{23}$). ^h Estimated from the delayed fluorescence³⁹ and magnetic field effect⁴⁰ experiments at room temperature. Any slowness^{16,39–41} in the nuclear relaxation of the instantaneous ΔG_{13} to its equilibrium value is not taken into account.

the calculated results of the uncertainty in model parameters and the validity of some approximations are discussed in several appendices.

2. Model

2.1. Kinetic Equations. We consider the kinetic scheme given in Figure 1. For this two-step model it leads to the following equations:

$$\frac{\mathrm{d}}{\mathrm{d}t}P_{1}(t) = -(k_{10} + k_{12})P_{1}(t) + k_{21}P_{2}(t), \tag{2.1}$$

$$\frac{\mathrm{d}}{\mathrm{d}t}P_2(t) = k_{12}P_1(t) - (k_{20} + k_{21} + k_{23})P_2(t) + k_{32}P_3(t),$$
(2.2)

$$\frac{\mathrm{d}}{\mathrm{d}t}P_3(t) = k_{23}P_2(t) - (k_{30} + k_{32} + k_{34})P_3(t). \tag{2.3}$$

Here, $P_1(t) \equiv [^1P*BH](t)$, $P_2(t) \equiv [P^+B^-H](t)$, and $P_3(t) \equiv [P^+BH^-](t)$ are the population densities of these distinct states. The k_{ij} 's are the rate constants defined in Figure 1.

Numerical estimates for the k_{ij} values and the associated free energy gaps ΔG_{ii} in Figure 1 for RCs of photosynthetic bacteria such as Rb. sphaeroides and Rps. viridis at zero external electric field are listed in Table 1. All of the free energy gaps ΔG_{ii} are assumed to be independent of temperature in the present analysis. The rate constants k_{10} , k_{20} , and k_{30} are assumed (initially) to be independent of temperature and electric field. (The electric field dependence of k_{10} and k_{20} will be considered in appendix C in relation to the fluorescence quantum yield.) The electric field and temperature dependences of the rate constants k_{12} , k_{21} , k_{23} , and k_{32} are described in terms of a nonadiabatic expression in section 2.3. For the quinone (Q)reduction ET rate constant k_{34} , two types of calculations are performed as follows: For the case of randomly oriented samples, $k_{34} = (200 \text{ ps})^{-1} 17,25$ is used, and later an estimate is made of the effect of varying it. For the case of oriented samples, we explicitly take into account an electric field dependence of k_{34} on the basis of a model in section 2.3 and compare the calculated results with those obtained for the fixed k_{34} . The back rate constant k_{43} is neglected since the associated free energy gap, $-\Delta G_{34}$, is much larger⁴² than the thermal energy k_BT even at room temperature and is estimated to

TABLE 2: Magnitude and Orientation of Dipole Moments of Radical Pairs Estimated from X-ray Diffraction Analyses²⁻⁷ for Photosynthetic RCs

species	magnitude (D)	orientation
$\mu(P^+B^-H)$ $\mu(P^+BH^-)$	51	а
$\mu(P^+BH^-)$	82	b
$\mu(P^+BHQ^-)$	134	c

^a Aligned by 77° with the pseudo- C_2 axis of the RC. ^b Aligned by 48° with the pseudo- C_2 axis of the RC and by 37° with μ (P+B-H). ^c The component projected onto the pseudo- C_2 axis of the RC is estimated to be 120 D.

continue to be much larger in the presence of the applied external fields discussed in the present study (cf. Figure 3b).

The free energy of a radical pair with the dipole moment μ in a RC is perturbed by an amount $-\mu \cdot \mathbf{F}_{\text{int}}$ in the presence of an applied external electric field \mathbf{F}_{ext} . Here, \mathbf{F}_{int} denotes the internal (partly induced) electric field experienced by the dipole. This field—dipole interaction causes a change in the free energy gap for the reaction $i \rightarrow j$,

$$\Delta G_{ii}(\mathbf{F}_{ext}) - \Delta G_{ii}(0) = -\Delta \boldsymbol{\mu}_{ii} \cdot \mathbf{F}_{int}, \qquad (2.4)$$

where $\Delta \mu_{ij}$ is the difference in dipole moment vectors of the pertinent ion pair states. The magnitude and orientation of the dipole moments of radical pairs, estimated from the X-ray diffraction analyses at atomic resolution for the RCs from *Rps. viridis*²⁻⁴ and *Rb. sphaeroides*, ⁵⁻⁷ are listed in Table 2. We assume $|\mu(^1P*BH)| \cong 0$ for simplicity initially, though this approximation is easily removed, and indeed, we include the magnitude of this dipole moment in the calculation in appendix C.

The internal field, \mathbf{F}_{int} , experienced by the dipoles in RCs is generally somewhat different from the externally applied field, \mathbf{F}_{ext} , because of the polarization of the surrounding medium. They are related by

$$\mathbf{F}_{\text{int}} = f \mathbf{F}_{\text{ext}}.\tag{2.5}$$

The local field correction f is assumed here to be a scalar constant, which is set equal to 1.2 as a standard value. 27,29,32,33 (The expression for f is considered in appendix B.)

2.2. Simplified (Quasi-Equilibrium) Approach. Although the results are given in a later section for the full solution of the kinetic equations 2.1–2.3, with and without an estimate of heterogeneity ^{12,15,35} of the samples, we first consider a highly simplified approximation which provides a simple analytical result for oriented samples and some insight into the quantum yield of the charge-separated state, in qualitative agreement with the lengthier solution of the complete equations.

The basic idea of the simplified approach is to note that certain rate constants are relatively large and to use them to obtain a quasi-equilibrium solution, P_i^e , which roughly approximates the behavior at intermediate reaction times. These relative concentrations are then used to calculate yields: Setting $dP_i/dt = 0$ in eqs 2.1–2.3 and neglecting k_{10} , k_{20} , k_{30} , and k_{34} during the above time regime, we obtain the equilibrium relations (see also appendix A):

$$P_1^{\rm e} = P_3^{\rm e} \exp(\beta \Delta G_{13}),$$
 (2.6)

$$P_2^{\rm e} = P_3^{\rm e} \exp(\beta \Delta G_{23}).$$
 (2.7)

Here, $\beta = (k_{\rm B}T)^{-1}$, $k_{\rm B}$ being the Boltzmann constant and T the absolute temperature, and $\Delta G_{13} = \Delta G_{12} + \Delta G_{23}$. Equations 2.6 and 2.7 are, of course, applicable irrespective of the values of rate constants.

The states ${}^{1}P^{*}BH$, $P^{+}B^{-}H$, and $P^{+}BH^{-}$ decay into the PBH and $P^{+}BHQ^{-}$ states with the rate constants k_{10} , k_{20} , k_{30} , and k_{34} , as in Figure 1. We thus obtain an approximate expression for the quantum yield of the charge-separated state $P^{+}BHQ^{-}$ as

$$Y_{\rm Q} \approx \frac{k_{34}P_{3}^{\rm e}}{k_{10}P_{1}^{\rm e} + k_{20}P_{2}^{\rm e} + (k_{30} + k_{34})P_{3}^{\rm e}}$$
 (2.8)

using eqs 2.6 and 2.7.

Using the values in section 2.1 and eqs 2.4–2.8, the calculated electric field (F_{ext}) dependence of the charge-separation quantum yield Y_0 for an oriented RC sample at T = 295 K is given in Figure 2a for the simplified model of this section, neglecting any effect of heterogeneity^{12,15,35} of the samples. For comparison between the experimental results²² using multilayer Langmuir-Blodgett (LB) films and the calculated results for an oriented system, we have assumed that the external electric field is parallel to the pseudo- C_2 axis of the RC (see section 3.1). Compared with the estimate for $Y_{\rm O}(F_{\rm ext})$ based on eq 1.1, even the simplified model, with and without the field dependence of k_{34} , is seen in Figure 2a for the oriented system to provide a significant improvement over eq 1.1 in reproducing the experimental QYE. We also show in Figure 2b the correspondingly calculated results based on the superexchange ET model (cf. appendix A). Some justification for the simplified analytical model and its utility for understanding the mechanism of the electric field effect are also addressed in appendix A.

2.3. Full Kinetic Approach. We proceed next to the full treatment of the rate eqs 2.1–2.3. To this end, it is necessary to evaluate the electric field dependence of several ET rate constants explicitly. In addition, the effect of including a static heterogeneity^{12,15,35} associated with the distribution of free energy gaps is also described. In this calculation we first neglect possible effects of the electric field on state mixing^{43–45} of ¹P* with other electronic configurations of P (cf. section 3.3.3).

With the initial condition of $P_1(0) = 1$ and $P_2(0) = P_3(0) = 0$, the rate eqs 2.1–2.3 can be solved to yield²¹

$$P_1(t) = \langle \sum_{j=1}^{3} A_j^{(1)} \exp(-t/\tau_j) \rangle,$$
 (2.9)

$$P_2(t) = \langle \sum_{j=1}^{3} A_j^{(2)} \exp(-t/\tau_j) \rangle,$$
 (2.10)

$$P_3(t) = \langle \sum_{i=1}^{3} A_j^{(3)} \exp(-t/\tau_j) \rangle.$$
 (2.11)

There is a distribution of the lifetimes τ_j and the amplitudes $A_j^{(i)}$ due to the distribution in k_{12} , k_{21} , k_{23} , and k_{32} (*vide infra*), and the brackets represent the average over the distribution.

The population density of the charge-separated state P⁺BHQ⁻ is then expressed as

$$P_4(t) = k_{34} \int_0^t dt' \, P_3(t') = k_{34} \langle \sum_{j=1}^3 A_j^{(3)} \tau_j [1 - \exp(-t/\tau_j)] \rangle.$$
(2.12)

The quantum yield of the charge-separated state P⁺BHQ⁻ is given accordingly by

$$Y_{Q} = P_{4}(\infty) = k_{34} \langle \sum_{j=1}^{3} A_{j}^{(3)} \tau_{j} \rangle.$$
 (2.13)

In addition, we define a $P_5(t)$ to describe the sum of internal

conversion and fluorescence of ${}^{1}P^{*}BH$ and a $P_{6}(t)$ to describe the charge recombination of $P^{+}B^{-}H$:

$$P_5(t) \equiv k_{10} \int_0^t dt' \, P_1(t') = k_{10} \langle \sum_{j=1}^3 A_j^{(1)} \tau_j [1 - \exp(-t/\tau_j)] \rangle, \tag{2.14}$$

$$P_6(t) \equiv k_{20} \int_0^t dt' \, P_2(t') = k_{20} \langle \sum_{j=1}^3 A_j^{(2)} \tau_j [1 - \exp(-t/\tau_j)] \rangle.$$
(2.15)

The combined quantum yield for the internal conversion and fluorescence of the singlet excited state ¹P*BH is then given by

$$Y_{\rm d} = P_5(\infty) = k_{10} \langle \sum_{j=1}^3 A_j^{(1)} \tau_j \rangle.$$
 (2.16)

As has been discussed extensively in the literature, $^{19,22-34}$ the field-induced change in the free energy gaps modifies the associated ET rate constants according to the standard ET theory. 46 In the present analysis, the ET rate constants for $^{1}P^*BH \rightarrow P^+B^-H$ (k_{12}), $P^+B^-H \rightarrow P^+BH^-$ (k_{23}), and $P^+BH^- \rightarrow P^+BHQ^-$ (k_{34}) are described in terms of a nonadiabatic expression incorporating the low-frequency medium vibrational modes characterized, for simplicity, by an average frequency $\omega_{\rm m}$ and the high-frequency intramolecular vibrational modes characterized by an average frequency $\omega_{\rm c}$: 21,47

$$k = \frac{2\pi V^2}{\hbar^2 \omega_{\rm m}} \exp[-S_{\rm m}(2\bar{\nu}_{\rm m} + 1)] \times \\ \exp(-S_{\rm c}) \sum_{n=0}^{\infty} \frac{S_{\rm c}^n}{n!} \left(\frac{\bar{\nu}_{\rm m} + 1}{\bar{\nu}_{\rm m}}\right)^{p(n)/2} \times I_{|p(n)|} (2S_{\rm m}[\bar{\nu}_{\rm m}(\bar{\nu}_{\rm m} + 1)]^{1/2}).$$
(2.17)

Here, V denotes the electronic coupling constant between the associated donor and acceptor; $S_{\rm m}=\lambda_{\rm m}/\hbar\omega_{\rm m},\ \lambda_{\rm m},\ {\rm and}\ \bar{\nu}_{\rm m}=[\exp(\beta\hbar\omega_{\rm m})-1]^{-1}$ refer to the reorganization energy and thermal population of the medium modes, respectively. $S_{\rm c}$ is the scaled reorganization constant $\lambda_{\rm c}/\hbar\omega_{\rm c}$ for the intramolecular modes, $I_{\nu}(z)$ is the modified Bessel function of order ν , and $p(n)\equiv (-\Delta G-n\hbar\omega_{\rm c})/\hbar\omega_{\rm m}$. The back ET reaction rate constants are then calculated using the detailed balance relation:

$$k_{ji} = k_{ij} \exp(\beta \Delta G_{ij}). \tag{2.18}$$

For room temperature, eq 2.17 reduces to⁴⁷

$$k = \frac{2\pi}{\hbar} V_2 \left(\frac{1}{4\pi \lambda_{\rm m} k_{\rm B} T} \right)^{1/2} \exp(-S_c) \sum_{n=0}^{\infty} \frac{S_c^n}{n!} \times \exp\left[-\frac{(\Delta G + \lambda_{\rm m} + n\hbar \omega_c)^2}{4\lambda_{\rm m} k_{\rm B} T} \right], (2.19)$$

since $k_{\rm B}T \gg \hbar \omega_{\rm m}$.

The values of the parameters^{21,42} used to calculate the rate constants k_{ij} are listed in Table 3. The values of the electronic coupling constants V_{ij} have been calculated such that the experimental ET rates¹⁷ at T = 295 K, $k_{12} = (2.3 \text{ ps})^{-1}$, $k_{23} = (0.9 \text{ ps})^{-1}$, and $k_{34} = (200 \text{ ps})^{-1}$ are reproduced using eq 2.19. We neglect in Table 3 the effects of changes in the parameters

TABLE 3: Parameters Used for the Calculation of ET Rate Constants k_{ii}

reaction $(i \rightarrow j)$	$\omega_{\rm m}{}^a$ (cm ⁻¹)	$\lambda_{\rm m}^b$ (cm ⁻¹)	$\omega_{\rm c}^{\ c}$ (cm ⁻¹)	$S_{ m c}{}^d$	V_{ij}^{e} (cm ⁻¹)	ref
$1 \rightarrow 2$	95	800	1500	0.5	32 ^f	21
$2 \rightarrow 3$	95	800	1500	0.5	59 ^f	21
$1 \rightarrow 3^g$		1600	1500	0.5	29^{h}	21
$3 \rightarrow 4$		4800	1600	1.0	4.8	42

^a Characteristic frequency for the medium's low-frequency vibrational modes. b Reorganization energy of the medium's low-frequency vibrational modes. ^c Characteristic frequency for the intramolecular high-frequency vibrational modes. ^d Scaled reorganization constant, λ_{c} $\hbar\omega_{\rm c}$, for the intramolecular high-frequency vibrational modes. ^e Elecronic coupling constant which reproduces the experimental ET rate constant k_{ij} (Table 1) at $F_{\text{ext}} = 0$ and T = 295 K using eq 2.19. ^f These values for V_{ij} , obtained by a fitting to data on rates and approximate energies, are close to those obtained by a fitting in ref 21, which gave the values of $V_{12} = 26 \text{ cm}^{-1}$ and $V_{23} = 51 \text{ cm}^{-1.48}$ The minor differences are due, in part, to their k_{ij} values²¹ being somewhat lower than ours and do not affect any of the conclusions.⁴⁹ g Used only for the calculation of k_{13} in Figure 2b. ^h Value at $F_{\text{ext}} = 0$ which yields k_{13} = $(3.2 \text{ ps})^{-1}$ at T = 295 K using eq 2.19. Only this quantity depends on the applied electric field through its dependence on the free energy gaps, 18,19,29 which causes the reduction in the quantum yield Y_0 based on eq 1.1 for $F_{\text{ext}} > 0$ observed in Figure 2b.

due to changes in temperature, volume, and electric field, except in the superexchange electronic coupling constant V_{13} .

It has been pointed out 12,15 that there may exist experimentally a distribution of free energies of the ion pair states P⁺B⁻H and P⁺BH⁻ due to any static heterogeneity in RCs. To explain the detailed magnetic field and temperature dependences of the recombination dynamics of the radical pair P⁺BH⁻ in transient absorption and delayed emission, Ogrodnik et al.35 described the heterogeneity of the energy of this ion pair state in terms of a Gaussian distribution of the free energy gap ΔG_{13} (= ΔG_{12} + ΔG_{23}) with the variance $\sigma_{13} = 400 \text{ cm}^{-1}$. Taking account of their result, we assume that the free energy gaps ΔG_{12} and ΔG_{23} are distributed about the mean values ΔG_{12} and ΔG_{23} , respectively, according to a following probability density:²¹

$$p(\Delta G) = \left(\frac{1}{2\pi\sigma^2}\right)^{1/2} \exp\left[-\frac{(\Delta G - \overline{\Delta G})^2}{2\sigma^2}\right]. \quad (2.20)$$

Here, ΔG_{12} and ΔG_{23} are set equal to the values calculated from Tables 1 and 2 without inclusion of any heterogeneity, and the corresponding variances are approximated as $\sigma_{12} = \sigma_{23}$ = $\sigma_{13}/\sqrt{2}$ with σ_{13} = 400 cm⁻¹. (We assume, thereby, for simplicity that $\sigma_{13}^2 = \sigma_{12}^2 + \sigma_{23}^2$ (independent events) and that σ_{13}^2 is equally divided between σ_{12}^2 and σ_{23}^2 .) For the other free energy gaps listed in Table 1, we do not include any effect of the heterogeneity. Thus, in the present kinetic model, the values of ET rate constants, k_{12} , k_{21} , k_{23} , and k_{32} , are distributed about their mean values, due to any static inhomogeneity and, in the case of randomly oriented samples, due also to a random distribution in the relative orientation between the dipoles and the applied field.³⁴

On the basis of the kinetic model defined above, the temporal variations of the population densities and the final quantum yields are calculated as functions of applied electric field, and the physical implications of the results are discussed in the following. No special techniques were needed for solving eqs 2.1-2.3, since the characteristic equation for them is cubic and can be solved analytically. Even for the most complicated calculation (a quantum-mechanical calculation for the randomly oriented systems, including static heterogeneity) the numerical programming was straightforward.

3. Results and Discussion

3.1. Oriented Systems. Using multilayer LB films of RCs from the photosynthetic bacterium Rb. sphaeroides, Popovic et al.²² measured the electric field dependence of the (absolute value of) quantum yield of charge separation at room temperature in terms of the light-induced voltage generated across the films. The system here contained the quinone (Q). In their experiments, it was supposed²² that the RC is fully (or at least partially) oriented and that the electric field is applied approximately in parallel with the pseudo- C_2 axis of the RC. They found that the quantum yield of P⁺BHQ⁻ formation decreases from a value of 0.96 at zero applied field to about 0.75 for a field of 1.2 MV/cm that is vectorically directed to hinder the charge separation. A plot of their results is given in Figure 2 and later in Figure 5.

In order to compare with these data, we have performed the calculation for the full kinetic model prescribed in section 2.3. The external electric field, F_{ext} , is assumed to be parallel to the pseudo- C_2 axis of the RC. The positive direction of the field has been defined such that the free energies of the ion pairs, P⁺B⁻H, P⁺BH⁻, and P⁺BHQ⁻, decrease due to the field—dipole interaction (i.e., the field is defined as positive when directed from the non-heme Fe to the bacteriochlorophyll dimer P).²² The temperature has been fixed at T = 295 K, and we therefore used eq 2.19 for the calculation of k_{12} , k_{23} , and k_{34} . The adequacy of using eq 2.19 instead of eq 2.17 was confirmed by comparison of the two calculated values for the ET rate constants at a number of values of the free energy gaps.

In Figure 3a the calculated electric field dependence of the ET rate constants, k_{12} , k_{21} , k_{23} , and k_{32} , is depicted for -1.5 $MV/cm \le F_{ext} \le 1.5 MV/cm$, when the mean values of the free energy gaps, ΔG_{12} and ΔG_{23} , are introduced, for comparison, into eq 2.19. The relations $k_{12} > k_{21}$, $k_{23} > k_{32}$, and k_{12} , $k_{23} > (5 \text{ ps})^{-1}$ are obeyed in this parameter region. The first two inequalities imply that ΔG_{12} and $\Delta G_{23} \leq 0$ for all values of F_{ext} . The last inequality, which implies a relatively weak dependence of the forward ET rate constants on the applied electric field, explains why it was difficult to describe in earlier work the extent of the experimental charge-separation QYE by considering only the competition between the internal conversion plus fluorescence rate constant k_{10} (=(190 ps)⁻¹) of ¹P*BH and the forward ET rate constants k_{12} and k_{23} (cf. Figure 2). We also note that the position of the maximum in k_{12} and k_{23} in Figure 3a reflects the relationship between the free energy gap ΔG at $F_{\rm ext} = 0$ and the reorganization energy $\lambda_{\rm m}$, namely, - $\Delta G_{12} < \lambda_{\rm m}$ (normal region) for k_{12} and $-\Delta G_{23} > \lambda_{\rm m}$ (inverted region) for k_{23} . The shoulder for k_{23} at $F_{\rm ext} \simeq 0.9$ MV/cm corresponds to $\Delta G_{23} + \lambda_{\rm m} + \hbar \omega_{\rm c} \simeq 0$ (cf. eq 2.19), which would therefore become more gradual if the distribution of the high-frequency modes (ω_c) were taken into account.

It was suggested by Moser et al.23 that the absence of an electric field effect on the initial step in oriented systems is consistent with a sequential ET model but not with a superexchange model. We have made calculations for both models, and the effect on the forward ET rate constant $k_{\rm et}$ is seen to be small for the sequential model (Figures 2a and 3a) and substantial for the superexchange model (Figure 2b), at least for the free energy values used. The initial rate constant for the disappearance of ${}^{1}P^{*}$ by the sequential model is $k_{12} + k_{10}$, i.e., essentially k_{12} . In Figure 3a it is seen that at $F_{\rm ext} = +0.8$ MV/cm the k_{12} increases by 15%, while at $F_{\text{ext}} = -0.8$ MV/cm it decreases by 20%. These figures are not inconsistent with the estimates, which had large error bars, made in ref 23.

In Figure 3b a calculated electric field dependence of k_{34} is similarly illustrated for these oriented systems. Reflecting the

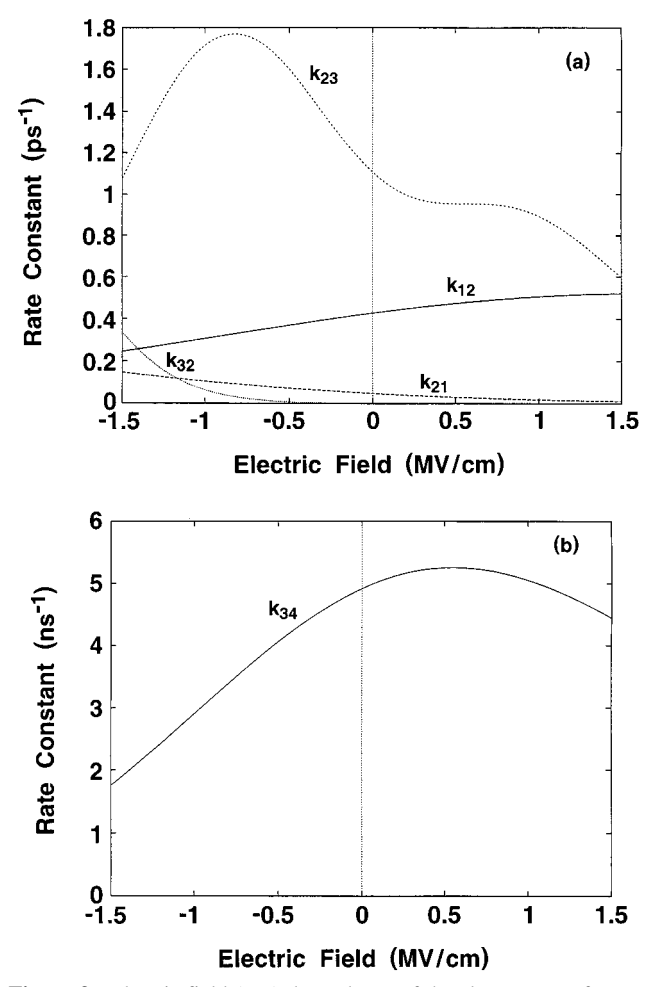


Figure 3. Electric field ($F_{\rm ext}$) dependence of the electron transfer rate constants calculated using eq 2.19 for an oriented system at T=295 K: (a) k_{12} , k_{21} , k_{23} , and k_{32} ; (b) k_{34} . (The back reaction rate constant k_{43} cannot be discerned from the abscissa.) For the sake of illustration, any effect of static heterogeneity is omitted here.

nearly activationless $(-\Delta G_{34} \simeq \lambda_{\rm m})$ property of the ET reaction and also the contribution of the high-frequency quantum modes $(\omega_{\rm c})$, the electric field dependence of k_{34} is not pronounced. The magnitude of the back ET rate constant, k_{43} , which is virtually indiscernible from the abscissa in Figure 3b, is negligible compared to the forward one k_{34} in this range of $F_{\rm ext}$.

In Figure 4a the behavior of the population densities $P_i(t)$ is shown as a function of the time elapsed after the photoexcitation of P, in the case of $F_{\rm ext}=0$. This figure is quite similar to that obtained by Schmidt $et~al.^{17}$ (Figure 2b in their paper), although their calculation did not incorporate any static heterogeneity. The population $P_2(t) = [P^+B^-H](t)$ has a maximum value $P_2^{\rm max} = 0.19$ at t = 1.4 ps, which is close to an approximate estimate, $P_2^{\rm max} \approx 0.21$, given by an expression:¹⁸

$$P_2^{\text{max}} \approx x^{1/(1-x)} \tag{3.1}$$

with $x \equiv k_{12}/k_{23}$, $k_{12} = (2.3 \text{ ps})^{-1}$, and $k_{23} = (0.9 \text{ ps})^{-1}$. The population $P_3(t) = [P^+BH^-](t)$ has a maximum value $P_3^{\text{max}} = 0.91$ at t = 14 ps, at which $P_1(t)$ and $P_2(t)$ have already decayed to nearly zero. Almost all electrons going to H at this time appear to move to Q, thus giving a high value of the quantum yield of P^+BHQ^- ($Y_Q = P_4(\infty) = 0.96$).

The calculated results for the population densities for the case of $F_{\rm ext} = -1.2$ MV/cm are depicted in Figure 4b. As compared with the case of $F_{\rm ext} = 0$, it is seen that $P_1(t)$ and $P_2(t)$ survive much longer with apparently multiple lifetimes.⁵⁰ It is particu-

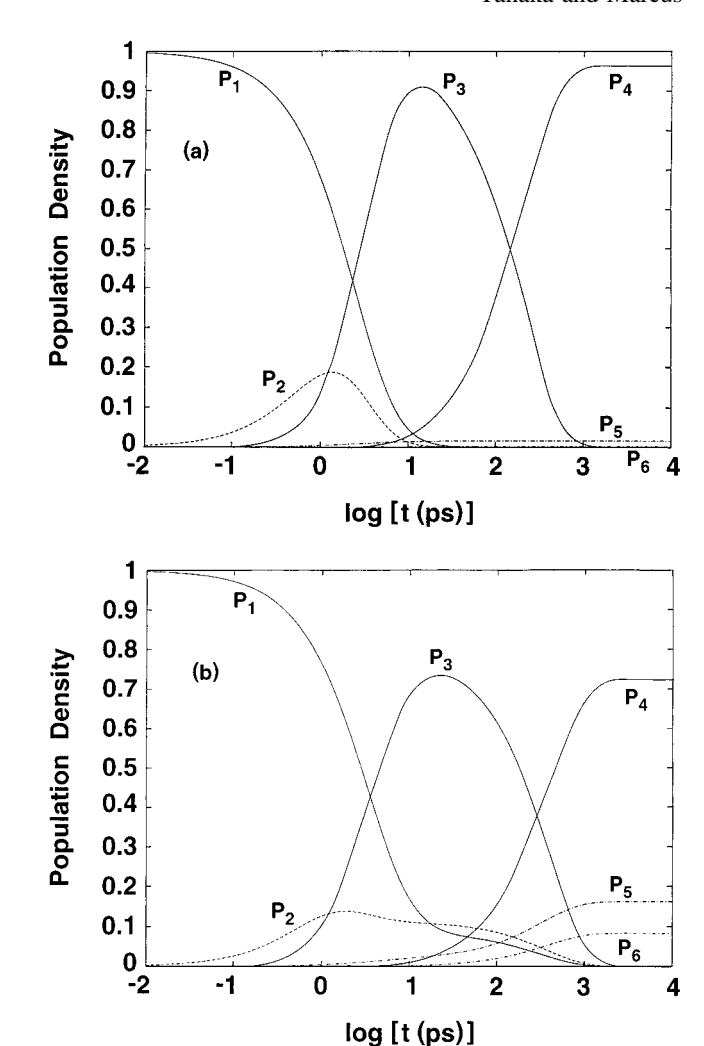


Figure 4. Time evolution of the population densities, $P_1(t) = [^1P^*BH]_{-}(t)$, $P_2(t) = [P^+B^-H]_{-}(t)$, $P_3(t) = [P^+BH]_{-}(t)$, $P_4(t) = [P^+BHQ^-]_{-}(t)$, $P_5(t) = k_{10} \int_0^t dt' P_1(t')$, and $P_6(t) = k_{20} \int_0^t dt' P_2(t')$, in the full kinetic model for an oriented system at 295 K with inclusion of the effect of static heterogeneity. The t denotes the time elapsed after the photoexcitation of the bacteriochlorophyll dimer: (a) at $F_{\rm ext} = 0$, (b) at $F_{\rm ext} = -1.2$ MV/cm.

larly seen that a steady state in which $P_1(t)$, $P_2(t)$, and $P_3(t)$ remain almost constant is approximately realized over the time period of $t \approx 10-100$ ps, which corresponds to the quasiequilibrium state mentioned in section 2.2 (see appendix A). If we estimate the characteristic time t_{st} for the occurrence of this steady-state as the time at which $P_3(t)$ attains its maximum value P_3^{max} , we find $t_{\text{st}} = 22$ ps. The values of the population densities, $P_1 = 0.09$, $P_2 = 0.11$, and $P_3 = 0.73$, at $t = t_{st}$, together with the magnitudes of the decay constants, k_{10} , k_{20} , and k_{34} , approximately govern the quantum yields, $Y_d = P_5(\infty)$, $P_6(\infty)$, and $Y_Q = P_4(\infty)$, respectively. Indeed, $P_5(\infty)$: $P_6(\infty)$: $P_4(\infty) = 0.22:0.12:1$ compares well with $k_{10}P_1(t_{st}):k_{20}P_2(t_{st}):$ $k_{34}P_3(t_{st}) = 0.28:0.12:1$. In this numerical solution we also obtain $Y_Q = 0.72$ for the quantum yield of P⁺BHQ⁻ at $F_{\text{ext}} =$ -1.2 MV/cm. It has been reduced from the value $Y_Q = 0.96$ at $F_{\text{ext}} = 0$, in accordance with the decrease of P_3^{max} . This behavior in $P_i(t)$ which governs the electric field effect on the quantum yields is well described in terms of the simplified quasiequilibrium approach in section 2.2, as will be illustrated in appendix A.

The calculated results for the dependence of the charge-separation quantum yield Y_Q on the electric field $F_{\rm ext}$ are shown by the solid curve in Figure 5. While the present model calculations can reproduce fairly well the overall behavior

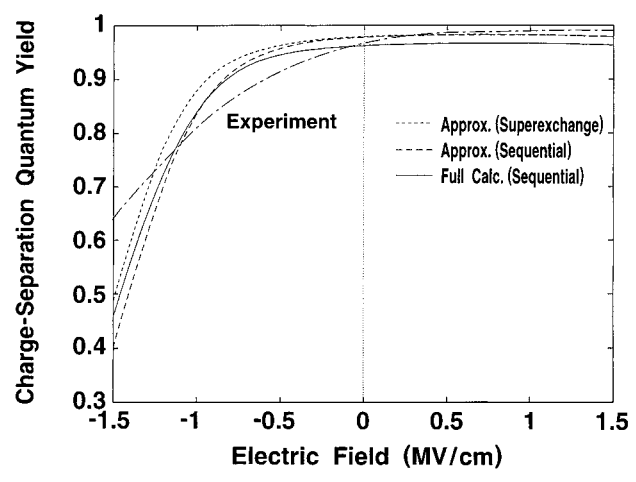
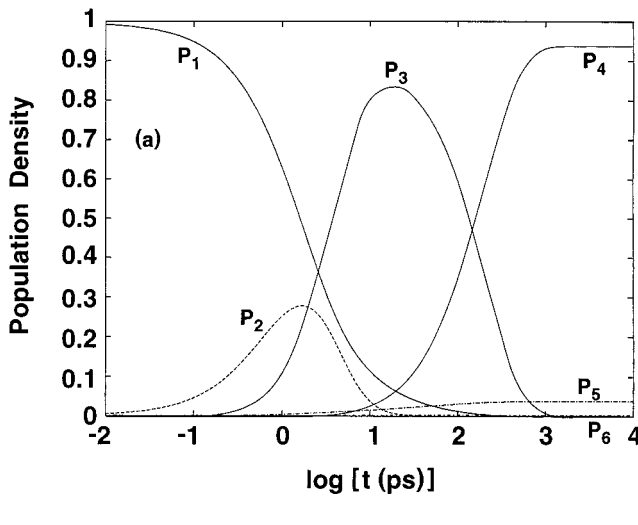


Figure 5. Electric field dependence of the charge-separation quantum yield Y₀ for an oriented system at 295 K. Solid curve: results obtained by solution of the rate equations for the full kinetic model given in section 2. Dashed and dotted curves: for the simplified model, values of $Y_0(F_{\text{ext}})$ based on eq 2.8 (sequential model) and eq A.16 (superexchange model), respectively. All the calculations include an effect of the heterogeneity for the free energy gaps, ΔG_{12} and ΔG_{23} , and an electric field dependence of k_{34} . Chain curve denotes the (fitted) experimental results.22

observed in the experiments by Popovic et al.²² (chain curve in Figure 5), any detailed comparison between theory and experiment depends, as one sees from Figures 10-12 in appendix B, on the uncertain values for the free energy gaps, the heterogeneity, and the local field correction, e.g., on model parameters such as ΔG_{23} , σ_{13} , and f.

3.2. Randomly Oriented Systems. The effect of an electric field on quinone (Q)-depleted RCs from Rb. sphaeroides embedded in polyvinyl alcohol (PVA) films was investigated by Ogrodnik et al.24 in picosecond transient absorption experiments. Upon application of a field of 0.7 MV/cm at 90 K, they observed a (relative) reduction of the quantum yield of P⁺BH⁻ by $11 \pm 1.5\%$ within the time resolution of their experiments, 30 ps. More recently, at T = 80 K Lao et al.²⁵ measured the field-induced QYE of formation of P+BH- (in Q-depleted samples) on a time scale of ~10 ns and of P+BHQ- on a time scale of \sim 10 ms using Rb. sphaeroides RCs in PVA films and glycerol-buffer glasses over a wide range of external electric fields. They observed a (relative) reduction of the quantum yields of P⁺BH⁻ (in Q-depleted samples) and P⁺BHQ⁻ by about 30% each at $F_{\rm ext} = 1.5$ MV/cm, indicating that the QYE for these samples at 80 K occurs regardless of any effect of Q on the charge-separation process. Since immobilized isotropically oriented samples are used in these experiments, the relative orientation between the applied field and the dipoles in the RCs is random. The free energy gaps, ΔG_{12} and ΔG_{23} , are therefore distributed depending on this relative orientation,³⁴ in addition to the distribution (assumed Gaussian) due to any static heterogeneity.

We have performed the calculations for the population densities and the quantum yields for these randomly oriented samples at T = 80 K, using the full kinetic model in section 2.3. Equation 2.17 was used for the calculation of k_{12} and k_{23} . The value of k_{34} was fixed at $(200 \text{ ps})^{-1}$, 17,25 and the effect of its variation is assessed in appendix B. The temporal variations of the population densities $P_i(t)$ at $F_{\text{ext}} = 0$ and 1.5 MV/cm are depicted in Figure 6. As in Figure 4, $P_1(t)$ and $P_2(t)$ at $F_{\text{ext}} =$ 1.5 MV/cm survive much longer than when $F_{\rm ext} = 0$, leading to a significant reduction in both P_3^{max} and Y_Q (= $P_4(\infty)$). The calculated results for the the relative charge-separation quantum yield, $Y_Q(F_{ext})/Y_Q(0)$, are shown in Figure 7 as a function of the applied electric field F_{ext} . In addition to the quantum-



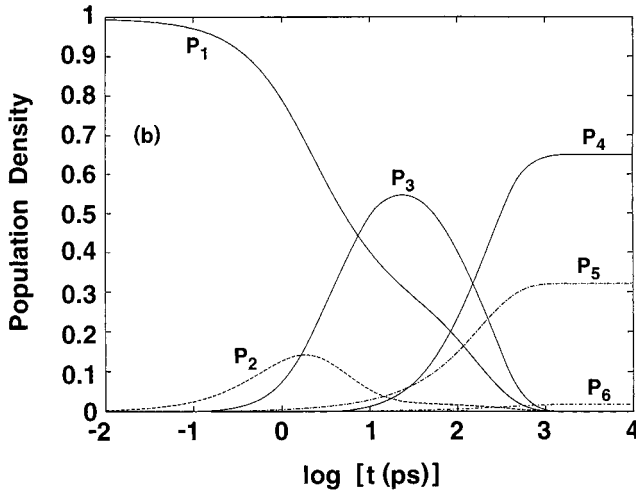


Figure 6. Time evolution of the population densities for a (Qcontaining) randomly oriented system at T = 80 K, calculated for the full kinetic model using eq 2.17 for k_{12} and k_{23} , and with $k_{34} = (200)$ ps)⁻¹: (a) at $F_{\text{ext}} = 0$, (b) at $F_{\text{ext}} = 1.5$ MV/cm. Otherwise, the symbols and the conditions are the same as those in Figure 4.

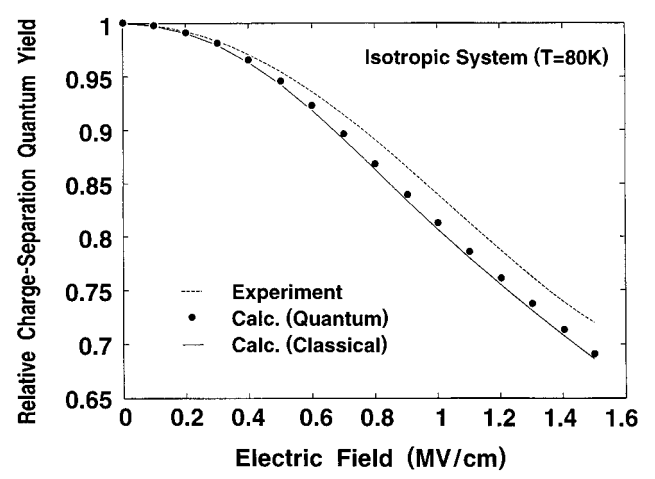


Figure 7. Electric field dependence of the relative quantum yield of charge separation, $Y_Q(F_{ext})/Y_Q(0)$, for the full kinetic model for a randomly oriented system at 80 K. Solid curve: results using the classical expression, eq 2.19, for the calculation of k_{12} and k_{23} . Solid circles: results obtained using the quantum expression, eq 2.17. Dashed curve: (fitted) experimental results.25

mechanical result, using $\omega_{\rm m} = 95~{\rm cm}^{-1}$ as a characteristic frequency of the medium vibrational modes, the plot also includes the classical result based on eq 2.19. The quantum effect on Y_Q with respect to the low-frequency medium vibrational modes is thus apparent but is seen to be very minor,

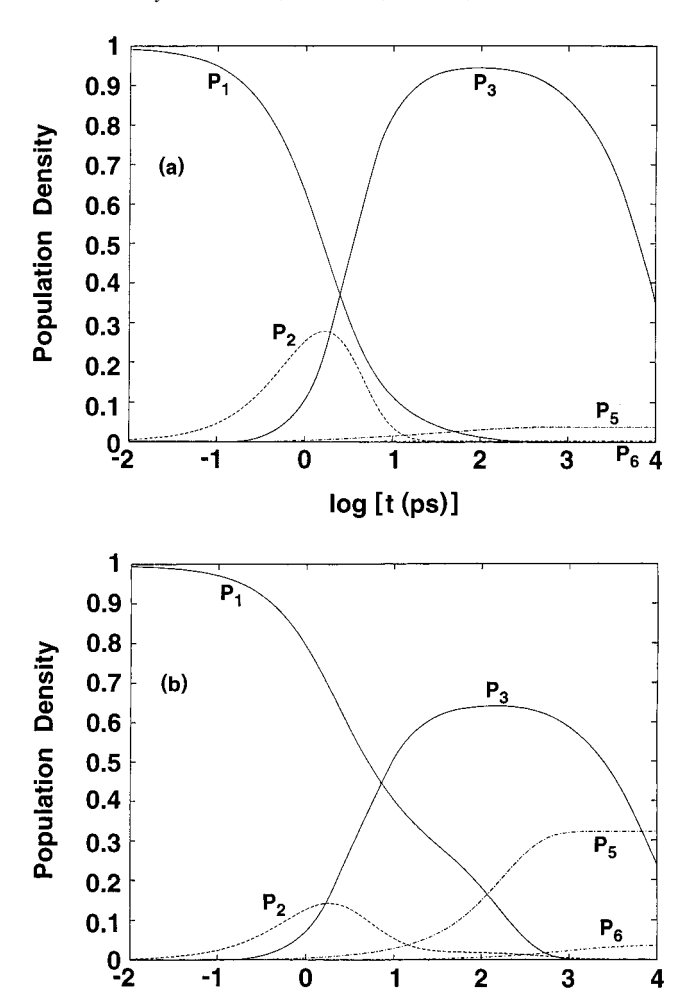


Figure 8. Time evolution of the population densities for a Q-depleted randomly oriented system at T = 80 K, calculated using the full kinetic model with $k_{34} = 0$: (a) at $F_{\rm ext} = 0$, (b) at $F_{\rm ext} = 1.5$ MV/cm. Otherwise, the symbols and the conditions are the same as those in Figure 6.

log [t (ps)]

even at this low temperature, T=80 K. (We note that even at 80 K a relevant quantity, 51 $\hbar\omega_{\rm m}/4k_{\rm B}T$, is less than unity, namely, 0.43.)

Because of the random distribution of the orientations, the centers of the distribution of ΔG_{12} and ΔG_{23} do not shift relative to the values they had without an external electric field. However, the field-induced QYE for the charge-separated state P^+BHQ^- is substantial owing to the contributions from those orientational regions of $\mathbf{F}_{\rm ext}$ which reduce the magnitudes of $|\Delta G_{12}|$ and $|\Delta G_{23}|$ (see also Figure 5 and discussion in appendix A). The calculated results for $Y_{\rm Q}(F_{\rm ext})/Y_{\rm Q}(0)$ approximately reproduce the experimental data, 25 denoted by the dashed line in Figure 7, recalling the uncertainties involved in the model parameters (cf. appendix B).

The maximum value of $P_3(t)$ at $t=t_{\rm st}$, $P_3^{\rm max}$, or, more accurately, $P_3(t_{\rm st})+P_4(t_{\rm st})$ in Figure 6 is approximately equal to the quantum yield of P⁺BH⁻, $Y_{\rm H}$, in the corresponding Q-depleted systems. It is found that $P_3^{\rm max}(F_{\rm ext})/P_3^{\rm max}(0)$ and $[P_3(t_{\rm st},F_{\rm ext})+P_4(t_{\rm st},F_{\rm ext})]/[P_3(t_{\rm st},0)+P_4(t_{\rm st},0)]$ equal 0.66 and 0.67, respectively, at $F_{\rm ext}=1.5$ MV/cm and agree well with $Y_{\rm Q}(F_{\rm ext})/Y_{\rm Q}(0)=0.69$. More explicitly, we also simulated in Figure 8 the population densities $P_i(t)$ for the Q-depleted randomly oriented systems at T=80 K and $F_{\rm ext}=0$ and 1.5 MV/cm, where we set $k_{34}=0$ in the full kinetic model to calculate the behavior in Q-depleted samples. The ratio $P_3(t,F_{\rm ext})/P_3(t,0)\equiv Y_{\rm H}(t,F_{\rm ext})/Y_{\rm H}(t,0)$ at $F_{\rm ext}=1.5$ MV/cm takes values of 0.62, 0.68, 0.68, and 0.66 at $t=10,10^2,10^3$, and 10^4

ps, respectively, which confirms that $Y_{\rm H}(F_{\rm ext})/Y_{\rm H}(0) \approx Y_{\rm Q}(F_{\rm ext})/Y_{\rm Q}(0)$. These results explain the experimental fact^{24,25} that the Q-containing samples and, on the experimental time scale of 10 ps to 10 ns, the Q-depleted samples show a similar effect of electric field on the quantum yields $Y_{\rm Q}$ and $Y_{\rm H}$, respectively.

3.3. Further Remarks. 3.3.1. Mechanism of the Electric Field Effect. As mentioned above and as demonstrated in Figures 2, 5, and 7, the experimental results for the effect of the electric field on the charge-separation quantum yield in bacterial photosynthetic RCs can be explained approximately in terms of the kinetic model given in section 2. In order to understand the charge-separation QYE, we conclude that special attention should be paid to the hierarchy among the rate constants, the consequent occurrence of an approximate steady state at $t \sim 10-100$ ps, and the role played by the back reactions: Not only the forward ET rate constants, k_{12} and k_{23} , but also the ones for the back reactions, k_{21} and k_{32} , play an important role for the determination of quantum yields. That is, as seen above, the quantum yields are governed not only by the forward ET rate constants but also by the free energy gaps, ΔG_{12} and ΔG_{23} . This new emphasis appears to overcome, in part, one difficulty in earlier models^{24,25,34} in which attempts were made to explain the charge-separation QYE in terms of eq 1.1. As seen in Figure 2, this latter approach leads to too small a theoretical QYE of charge separation when compared with experiment.

The numerical calculations for the full kinetic model also explain the experimental observation^{24,25} for randomly oriented systems at cryogenic temperatures that the Q-containing and Q-depleted samples showed a similar effect of electric field on the charge-separation quantum yields of P^+BHQ^- (Y_Q) and P⁺BH⁻ (Y_H), respectively. However, this fact does not necessarily imply that the Y_0 in the Q-containing system is always equal to the $Y_{\rm H}$ in the corresponding Q-depleted system: There would be a quantitative effect on Y_0 associated with the Q-reduction ET rate constant k_{34} , as suggested by eq 2.8 (i.e., $Y_{\rm O}$ versus $Y_{\rm H} \simeq P_{\rm 3}^{\rm e}$). This effect is more pronounced in the oriented system than in the randomly oriented system, as seen in Figures 13 and 14 in appendix B. To examine this theoretical prediction, it is interesting to experimentally explore the difference between the two (absolute) quantum yields, $Y_{\rm O}$ and $Y_{\rm H}$, in oriented samples as varying the values of k_{34} by applying electric fields and/or by using modified RCs.⁴²

3.3.2. Electric Field Effect on Fluorescence Quantum Yield. In addition to the charge-separation quantum yield, the calculations should also agree with the experimental studies^{27,28,30,31} made of the electric field effect on the fluorescence quantum yield Y_f inbacterial photosynthetic RCs. In the present model, a quantity related to the fluorescence quantum yield Y_f is the internal conversion plus fluorescence quantum yield, $Y_d = P_5(\infty)$, of the singlet excited state ¹P*BH. It is given by eq 2.16. The relevant rate constant k_{10} in Figure 1 can be written as a sum of the radiative (fluorescence) and nonradiative (internal conversion) rates,

$$k_{10} = k_{\rm r} + k_{\rm nr},\tag{3.2}$$

where $k_{\rm r}$ is known to be much smaller than $k_{\rm nr}$ (by about 1–2 orders of magnitude in the absence of an applied electric field). ^{27,41,42,52} The present kinetic model has assumed in the preceding sections that k_{10} (=(190 ps)^{-1 37}) is a constant, independent of the applied electric field; the main interest of this study was focused on the charge-separation quantum yield. If both $k_{\rm r}$ and $k_{\rm nr}$ are considered to be independent of the electric field, the fluorescence quantum yield,

obeys a relation,

$$\frac{Y_{\rm f}(F_{\rm ext})}{Y_{\rm f}(0)} = \frac{Y_{\rm d}(F_{\rm ext})}{Y_{\rm d}(0)}$$
(3.4)

In Figure 9 the electric field dependence of $Y_d(F_{ext})/Y_d(0)$ and hence of $Y_f(F_{ext})/Y_f(0)$ is shown for the randomly oriented system at 80 K. There, the quantum (eq 2.17) and classical (eq 2.19) expressions involving the low-frequency modes have been used in the calculation of the ET rate constants, k_{12} and k_{23} . The calculated results give too large an electric field effect on the fluorescence, when compared with experiment. For example, experimentally^{27,28,30,31} an enhancement of fluorescence by somewhat less than a factor of 2 at $F_{\text{ext}} = 1 \text{ MV/cm}$ is observed,⁵³ whereas the calculated value is seen in Figure 9 to be a factor of 5.7 in the quantum case. Some modification of this factor is seen in appendix C, where, for instance, a field dependence of k_{nr} due to a change in the free energy gap between ¹P*BH and PBH with field is added, reducing the factor 5.7 to about 4 (including now the dipole moment difference between ¹P*BH and PBH). However, there still remains a substantial discrepancy, perhaps.

In this simplest version of the present model the enhancement of $[1 - Y_0(F_{ext})]/[1 - Y_0(0)]$ should approximately equal $Y_f(F_{ext})/Y_f(0)$. But experimentally the former was, assuming $Y_0(0) = 0.96$, a factor of about 5 at $F_{\text{ext}} = 1.0 \text{ MV/cm}$ in randomly oriented samples at 80 K,25 whereas the latter was only about $1.5-2.^{27,28,30,31}$ The inclusion, above, of the electric field dependence of k_{nr} means that in this improved model the enhancement of $[1 - Y_Q(F_{ext})]/[1 - Y_Q(0)]$ no longer has to equal $Y_f(F_{ext})/Y_f(0)$, but we have seen that there still is some discrepancy. (The factor of 1.5–2 should now be compared with the factor of about 4, instead of 5-6.) While one possible explanation of the remaining discrepancy would be that some of the samples are "dead" and so their fluorescence would be unaffected by an electric field, the fraction of dead samples at room temperature has been estimated for Rb. sphaeroides to be only about 15%.⁵⁴ So it is desirable to seek elsewhere for an explanation of the remaining discrepancy.

3.3.3. Electric Field Effect on Possible Mixing of States. The analysis given thus far does not, in fact, explain two particular experimental facts: (i) the fluorescence quantum yield Y_f is less affected than Y_0 by electric fields in the randomly oriented samples^{27,28,30,31} and probably by negative fields in the oriented samples and (ii) the charge-separation quantum yield $Y_{\rm O}$ increases in the oriented samples when the electric field is sufficiently positive(cf. Figures 2 and 5).22 One potential explanation for both points i and ii is that the electric field can affect the mixing of ¹P*BH with its nearby charge-transfer (CT) electronic states⁴³⁻⁴⁵ by modifying their energy difference: If the negative field enhances the mixing with this nearby state(s), the positive field would decrease the mixing in these oriented samples. Then, the Franck-Condon factor and hence the nonradiative rate constant k_{nr} could be enhanced in the former case and decreased in the latter. (The effective potential curve of the excited state would be expected to be more displaced from the ground state curve if CT states participated.) The decrease of k_{nr} in the positive electric field region would contribute to the increase of Y_0 according to the simple branching model. (We note that to increase Y_Q from 0.96 to 0.99^{22} requires a decrease of k_{nr} of a factor of about 4 if one neglects other factors such as the branching between k_{34} and k_{30} in Figure 1.) On the other hand, the increase of k_{nr} in the negative electric field region would contribute, together with

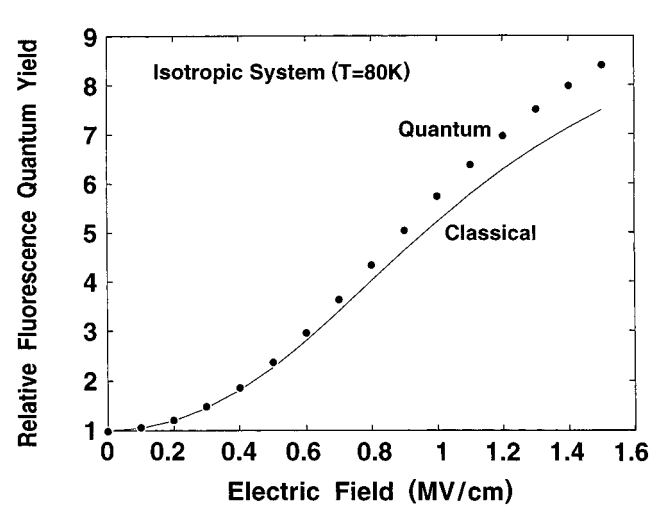


Figure 9. Electric field dependence of the relative quantum yield of radiative plus nonradiative decay of ${}^{1}P^{*}BH$ and $Y_{d}(F_{ext})/Y_{d}(0)$ and hence of the relative fluorescence quantum yield, $Y_{f}(F_{ext})/Y_{f}(0)$, for the full kinetic model for a randomly oriented system at 80 K. Solid curve: results in which the classical expression, eq 2.19, has been used for the calculation of k_{12} and k_{23} . Solid circles: results obtained using the quantum expression, eq 2.17.

the repopulation effect discussed in this paper, to the decrease of $Y_{\rm Q}$ there and also to a decrease of $Y_{\rm f}$ (cf. Figure 15a in appendix C) as opposed to the enhancement of $Y_{\rm f}$ by the repopulation effect. This effect may thus explain why the electric field effect on $Y_{\rm f}$ is less than that on $Y_{\rm Q}$ in the experiments.

3.3.4. Validity of the Nonadiabatic Approximation. In the analyses, we have calculated the primary ET rate constants, k_{12} and k_{23} , on the basis of the nonadiabatic expressions, eqs 2.17 and 2.19. Recalling that the fitted magnitudes of associated electronic coupling constants are fairly large ($V_{12} = 32 \text{ cm}^{-1}$ and $V_{23} = 59 \text{ cm}^{-1}$), a question may be raised as to whether one can rely on the nonadiabatic (golden rule) approximation or not, especially for k_{23} . This issue is addressed in appendix D.

4. Conclusions

In the present paper a theoretical model is proposed for the electric field effect on the charge-separation quantum yield in bacterial photosynthetic RCs. In previous models^{24,25,34} of the effect, the explanation for experimental results was based on a competition between the internal conversion plus fluorescence rate constant and the forward ET rate constant of ¹P*BH, *i.e.*, on eq 1.1, and led to too small a calculated effect (dotted line in Figure 2). In the present paper, the effect of the electric field on both the forward and the backward rate constants is incorporated, leading to a larger effect. The extent to which the calculated results depend on various parameters was also investigated.

The electric field effect on the fluorescence quantum yield in photosynthetic RCs was considered, and a mixing of $^{1}P^{*}$ with nearby CT states was invoked as a possible explanation of the experimental facts that the enhancement of $Y_{\rm f}(F_{\rm ext})/Y_{\rm f}(0)$ is much smaller than that of $[1-Y_{\rm Q}(F_{\rm ext})]/[1-Y_{\rm Q}(0)]$ in randomly oriented samples and that $Y_{\rm Q}(F_{\rm ext})$ increases for positive fields in oriented samples. The large polarizability of $^{1}P^{*}$, used to explain a large Stark effect, is consistent with this state mixing. 45

Acknowledgment. We thank Yuri Georgievskii, Antonio Hidalgo García, and Xueyu Song for useful discussions and Chao-Ping Hsu, Aseem Mehta, and Bryan Hathorn for their help in the preparation of the manuscript and the figures. S.T. acknowledges the financial support provided by Toshiba Corp.

during his stay at the California Institute of Technology. We are indebted to the National Science Foundation and the Office of Naval Research for the support of this research.

Appendix A: Approximate Analytical Model

Using the results of the numerical calculations for the full kinetic model, we give here some justification for the simplified quasi-equilibrium approach used in section 2.2. This analysis then provides some further insight into the mechanism of the electric field effect on the quantum yields in photosynthetic RCs.

In the kinetic scheme given in Figure 1, there is a hierarchy among the rate constants: Those associated with the primary ET reactions, k_{12} , k_{21} , and k_{23} , and, in the case of very negative $F_{\rm ext}$, in the oriented system, k_{32} , are much larger than the others. (One may compare the values of these k_{ij} 's shown in Figure 3a with those used for k_{10} , k_{20} , and k_{30} in Table 1 and with the k_{34} in Figure 3b.) As illustrated in Figure 3, this hierarchy seems to apply over a wide range of external electric fields. Accordingly, to obtain some insight into the importance of the $P_i^{\rm e}$'s in section 2.2, we can replace eqs 2.1-2.3 approximately by

$$\frac{\mathrm{d}}{\mathrm{d}t}P_{1}(t) = -k_{12}P_{1}(t) + k_{21}P_{2}(t),\tag{A.1}$$

$$\frac{\mathrm{d}}{\mathrm{d}t}P_2(t) = k_{12}P_1(t) - (k_{21} + k_{23})P_2(t) + k_{32}P_3(t), \quad (A.2)$$

$$\frac{\mathrm{d}}{\mathrm{d}t}P_3(t) = k_{23}P_2(t) - k_{32}P_3(t),\tag{A.3}$$

neglecting k_{10} , k_{20} , k_{30} , and k_{34} for times less than $t \sim 20$ ps. With the normalization condition of $P_1(t) + P_2(t) + P_3(t) = 1$, the solution at $t = \infty$ to the rate equations A.1–A.3 is given by

$$P_1(\infty) = \frac{k_{21}k_{32}}{k_{21}k_{32} + k_{12}k_{32} + k_{12}k_{23}},$$
 (A.4)

$$P_2(\infty) = \frac{k_{21}k_{32}}{k_{21}k_{32} + k_{12}k_{32} + k_{12}k_{23}},\tag{A.5}$$

$$P_3(\infty) = \frac{k_{12}k_{23}}{k_{21}k_{32} + k_{12}k_{32} + k_{12}k_{23}}.$$
 (A.6)

This solution can then be rewritten as

$$P_{1}(\infty) = \frac{\exp(\beta \Delta G_{13})}{\exp(\beta \Delta G_{13}) + \exp(\beta \Delta G_{23}) + 1}, \quad (A.7)$$

$$P_2(\infty) = \frac{\exp(\beta \Delta G_{23})}{\exp(\beta \Delta G_{13}) + \exp(\beta \Delta G_{23}) + 1}, \quad (A.8)$$

$$P_3(\infty) = \frac{1}{\exp(\beta \Delta G_{13}) + \exp(\beta \Delta G_{23}) + 1}$$
 (A.9)

with the aid of the detailed balance relation, eq 2.18. This solution for $P_i(\infty)$ is seen to be identical to the quasi-equilibrium solution P_i^e given in section 2.2.

In Figures 4b and 6b for the full calculation with the inclusion of static heterogeneity, the temporal regime, $t \sim 10-100$ ps, over which a steady state for $P_i(t)$ occurs approximately may be identified with the above quasi-equilibrium regime ($t = \infty$). In the case of an oriented system at $F_{\rm ext} = -1.2$ MV/cm and T = 295 K (Figure 4b), the ratios of the population densities of

¹P*BH, P⁺B⁻H, and P⁺BH⁻ are $P_1(t)$: $P_2(t)$: $P_3(t) = 0.13$:0.14:1 at $t = t_{st} = 22$ ps at which $P_3(t)$ has a maximum value.

It is useful, for comparison with this result of the full calculation for the oriented system, to incorporate the effect of the static heterogeneity in the simplified result, eqs 2.6-2.7 or A.7-A.9. Considering that this inhomogeneity in RCs causes additional fluctuations in the distribution of the free energy gaps in a way analogous to thermal fluctuations, a way of including this effect approximately for the quasi-equilibrium calculations is by replacing the thermal energy k_BT by effective values:

$$k_{\rm B}T' \equiv \sqrt{(k_{\rm B}T)^2 + \alpha \sigma_{13}^2} \equiv 1/\beta',$$
 (A.10)

$$k_{\rm B}T'' \equiv \sqrt{(k_{\rm B}T)^2 + \alpha \sigma_{23}^2} \equiv 1/\beta'',$$
 (A.11)

where α is a constant of the order of unity. Equations A.7—A.9 then lead to

$$P_1^{\rm e} = P_3^{\rm e} \exp(\beta' \overline{\Delta G_{13}}), \tag{A.12}$$

$$P_2^{\rm e} = P_3^{\rm e} \exp(\beta'' \overline{\Delta G_{23}}) \tag{A.13}$$

instead of eqs 2.6 and 2.7, which contain the free energy gaps $\overline{\Delta G_{ij}}$ without the heterogeneity. Employing $\alpha = 0.35^{55}$ for the oriented system and using $\overline{\Delta G_{12}} = -170 \text{ cm}^{-1}$, $\overline{\Delta G_{23}} = -500 \text{ cm}^{-1}$, and $\overline{\Delta G_{13}} = -670 \text{ cm}^{-1}$ at $F_{\text{ext}} = -1.2 \text{ MV/cm}$ (cf. Tables 1 and 2), we find $P_1^{\text{e}} \cdot P_2^{\text{e}} : P_3^{\text{e}} = 0.12 \cdot 0.15 \cdot 1$ from eqs A.10–A.13 for T = 295 K and $\sigma_{13} = 400 \text{ cm}^{-1}, ^{35}$ which is in good agreement with the above numerical result for the full calculation, $P_1(t_{\text{st}}) : P_2(t_{\text{st}}) : P_3(t_{\text{st}}) = 0.13 \cdot 0.14 \cdot 1$.

As seen in Figure 4b, after a steady or quasi-equilibrium state among ¹P*BH, P⁺B⁻H, and P⁺BH⁻ is realized at $t \sim 20$ ps, these states decay into the PBH and P+BHQ- states with the rate constants k_{10} , k_{20} , k_{30} , and k_{34} . An approximate expression for the quantum yield of the charge-separated state P+BHQ- is thus given by eq 2.8. For $F_{\text{ext}} = -1.2 \text{ MV/cm}$ and T = 295 K, eq 2.8 with inclusion of the heterogeneity gives $Y_Q = 0.71$, which is in good agreement with the numerical result of the full calculation, $Y_0 = 0.72$, found in section 3.1. Also shown, by a dashed curve in Figure 5, are the values of $Y_{\rm O}(F_{\rm ext})$ obtained from eqs 2.8, A.12, and A.13 for the case of an oriented system at 295 K. In spite of its simple form, eq 2.8 is seen in Figure 5 to reproduce the results of the solution to the full kinetic model in section 2.3 fairly well. The slight deviation between the solid and dashed curves in Figure 5 may be ascribed to the breakdown of the assumption of a steady state when k_{32} and k_{21} become too small (cf. Figure 3a) and also to an inadequacy of eqs A.10 and A.11 (cf. Figure 11 later).

In the text we used only the sequential model for the primary ET reactions in RCs, partly for brevity of presentation. It is useful, therefore, to give the analogous (approximate) calculation for the superexchange model: The superexchange ET step,

$${}^{1}P*BH \xrightarrow{k_{13}} P^{+}BH^{-},$$
 (A.14)

is considered instead of the sequential ET steps,

$${}^{1}P^{*}BH \xrightarrow{k_{12}} {}^{k_{12}}P^{+}B^{-}H \xrightarrow{k_{23}} {}^{k_{23}}P^{+}BH^{-},$$
 (A.15)

in the kinetic scheme of Figure 1. Using an analysis analogous to that leading to eqs 2.8, A.12, and A.13, we find

$$Y_{\rm Q} \approx \frac{k_{34}}{k_{10} \exp(\beta' \overline{\Delta G_{13}}) + k_{30} + k_{34}}$$
 (A.16)

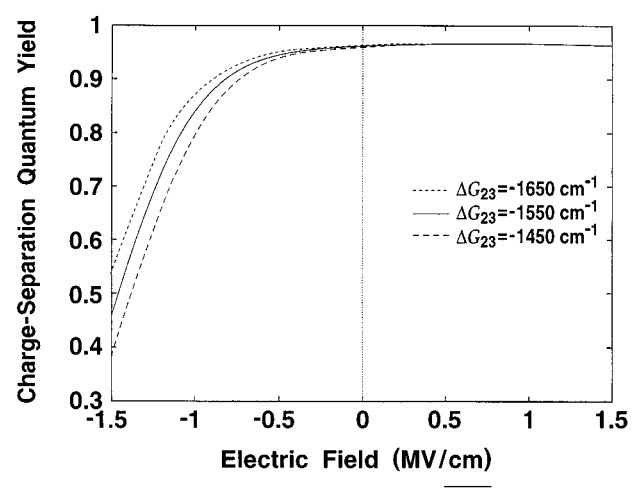


Figure 10. Influence of the free energy gap ΔG_{23} at $F_{\rm ext}=0$ on $Y_{\rm Q}(F_{\rm ext})$ for an oriented system at 295 K. Dashed, solid, and dotted curves: calculated results for the full kinetic model in which $\Delta G_{23} - 1450$, -1550, and -1650 cm⁻¹ at $F_{\rm ext}=0$ have been adopted, respectively. The electronic coupling constants, $V_{23}=57$, 59, and 61 cm⁻¹, have been used, respectively, to reproduce $k_{23}=(0.9 \text{ ps})^{-1}$ at $F_{\rm ext}=0$. The remaining conditions are the same as those in Figure 5.

for the superexchange ET model. The values of $Y_Q(F_{\rm ext})$ calculated from this expression are plotted as the solid (when k_{34} is field-independent) and dashed (when k_{34} is field-dependent) curves in Figure 2b (without the heterogeneity) and as the dotted curve in Figure 5 (with the field dependence of k_{34} and the heterogeneity). The results show that eq A.16 can describe the electric field effect on Y_Q at least qualitatively. However, some difficulties 18,19 in the superexchange ET model for describing the primary ET reactions in photosynthetic RCs have been noted (see also refs 21 and 36).

Appendix B: Influence of Parameter Uncertainties

We consider here how the calculated results for the charge-separation quantum yield Y_Q in section 3 are modified by varying the model parameters in section 2.

As seen in section 2.2 and appendix A, the values of $Y_Q(F_{\rm ext})$ should be dependent on the choices of the mean free energy gaps, ΔG_{12} and ΔG_{23} , and they have some experimental uncertainty. $^{16,21,39-41}$ In Figure 10 the dependence of the calculated values of $Y_Q(F_{\rm ext})$ on $\Delta G_{23}(F_{\rm ext}=0)$ is illustrated in the case of the oriented system at 295 K. Here, $V_{23}=57$ and 61 cm⁻¹ have been used for $\Delta G_{23}=-1450$ and -1650 cm⁻¹, respectively, in order to reproduce the same $k_{23}=(0.9 \text{ ps})^{-1}$ at $F_{\rm ext}=0$. The qualitative behavior of the $F_{\rm ext}$ dependence of Y_Q is seen to be the same for these ΔG_{23} 's, but there is a quantitative effect, as suggested by eqs 2.8, A.12, and A.13. 56 An analogous but smaller modification may be expected with the variation in ΔG_{12} . 57

The discussion in appendix A also suggests that the values of $Y_{\rm Q}(F_{\rm ext})$ may depend on the extent of the static heterogeneity of the free energy gaps. In Figure 11 the dependence of the calculated $Y_{\rm Q}(F_{\rm ext})$ on the values of $\sigma_{13}=\sqrt{2}\sigma_{12}=\sqrt{2}\sigma_{23}$ is depicted for the oriented system at 295 K. As expected from eqs 2.8 and A.10–A.13, but now using instead the full kinetic model, it is found that the increase in the heterogeneity σ makes the field dependence of the charge-separation quantum yield more gradual, just as an increase in temperature does. The calculated result for $\sigma_{13}=400~{\rm cm}^{-1}$ (the value estimated for randomly oriented RC samples³⁵) shows a steeper $F_{\rm ext}$ dependence of $Y_{\rm Q}$ than that actually observed in oriented samples²² as seen in Figure 5. While this result is consistent with the idea²⁵ that there may exist additional heterogeneity associated

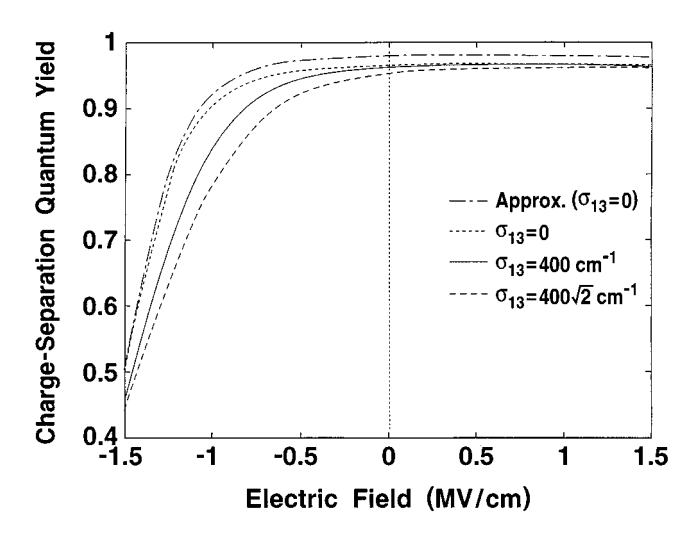


Figure 11. Influence of the heterogeneity σ_{13} on the calculated results of $Y_{\rm Q}(F_{\rm ext})$ in the full kinetic model for an oriented system at 295 K. Dotted curve: $\sigma_{13} = 0$. Solid curve: $\sigma_{13} = 400 \ {\rm cm^{-1}}$. Dashed curve: $\sigma_{13} = \sqrt{2} \times 400 \ {\rm cm^{-1}}$. Chain curve: approximate estimates based on eq 2.8 with $\sigma_{13} = 0$. The remaining conditions are the same as those in Figure 5.

with disorder in sample orientation and thickness in the LB films of RCs used in the experiments,²² this finding does not rule out other factors.

The calculated values of $Y_{\rm Q}(F_{\rm ext})$ also depend on the choice of the local field correction f, which was defined by eq 2.5 and tentatively set equal to $1.2^{27,29,32,33}$ in section 2. In the case of randomly oriented RC samples embedded in PVA films, the local field correction may be expressed as

$$f = \frac{9\epsilon_{\text{PVA}}\epsilon_{\text{RC}}}{(2\epsilon_{\text{PVA}} + \epsilon_{\text{RC}})(2\epsilon_{\text{RC}} + \epsilon') + 2(r'/r_{\text{RC}})^3(\epsilon_{\text{PVA}} - \epsilon_{\text{RC}})(\epsilon_{\text{RC}} - \epsilon')}$$
(B.1)

with the use of the spherical cavity approximation for the RC and chromophores. Here, ϵ_{PVA} , ϵ_{RC} , and ϵ' denote the dielectric constants of PVA, RC, and chromophores, respectively; r_{RC} and r' ($< r_{\text{RC}}$) represent the effective radii of RC and chromophores. Equation B.1 was obtained by solving the electrostatic boundary problem of two concentric spheres embedded in a medium and in a uniform electric field. The inner sphere has a dielectric constant ϵ' , the outer sphere ϵ_{RC} , and the medium ϵ_{PVA} . Noting that $r_{\text{RC}} \gg r',^{2-7}$ eq B.1 reduces to a formula assumed in ref 33:

$$f = \frac{3\epsilon_{\text{PVA}}}{2\epsilon_{\text{PVA}} + \epsilon_{\text{RC}}} \cdot \frac{3\epsilon_{\text{RC}}}{2\epsilon_{\text{RC}} + \epsilon'}.$$
 (B.2)

At T=80 K, if one chooses $\epsilon'=2$ and $\epsilon_{\text{PVA}}=\epsilon_{\text{RC}}=4,^{33}$ then f=1.2. For oriented RC samples using LB films, there is no PVA and so the first factor in eq B.2 is absent. If one uses $\epsilon'=2$ and $\epsilon_{\text{RC}}=4-8$ at room temperature, 33 then f=1.2-1.33. One difficulty which has been noted 32 in using this value of f for the experiments by Popovic $et\ al.^{22}$ is due to the inhomogeneity of the samples: Usually, as in the experiments by Lao $et\ al.^{25}$ the value of the externally applied field is estimated as

$$F_{\rm ext} = V_{\rm app}/d \tag{B.3}$$

by measuring the applied voltage $V_{\rm app}$ and assuming that in the present case the distance d between the electrodes is uniform.

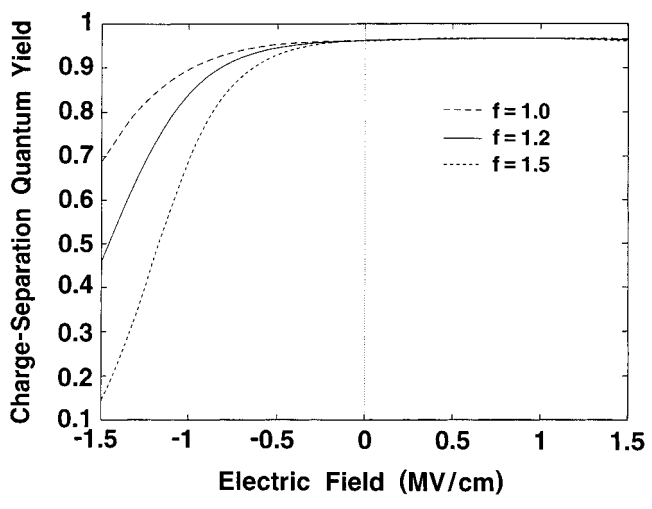


Figure 12. Influence of the local field correction f on the calculated results of $Y_{\rm Q}(F_{\rm ext})$ in the full kinetic model for an oriented system at 295 K. Dashed curve: f = 1.0. Solid curve: f = 1.2. Dotted curve: f = 1.5. The remaining conditions are the same as those in Figure 5.

Popovic et al., 22 instead, estimated the applied electric field as

$$F_{\text{ext}} = \frac{CV_{\text{app}}}{\epsilon_0 \epsilon_A A} \tag{B.4}$$

in terms of the sample cell area A, the capacitance C, and the dielectric constant of RC proteins ϵ_r , and they assumed ϵ_r to be 3. Here, ϵ_0 is the permittivity of vacuum. Equations B.3 and B.4 are related when one notes that $C = \epsilon_0 \epsilon A/d$, if the medium is assumed to be homogeneous, and if one then assumes $\epsilon =$ $\epsilon_{\rm r}$. It is ambiguous, however, how $\epsilon_{\rm r}$ is related to $\epsilon_{\rm RC}$ and ϵ' above. Thus, there are uncertainties in using eq B.3, which assumes constant d, or in using eq B.4, which makes an additional assumption but does not require that d be known. Accordingly, their estimate for F_{ext} (and consequently the value of f which should be used for model calculations) may contain some error and cause the comparison between theory and experiment to be less straightforward. In Figure 12 the calculated results of $Y_0(F_{\rm ext})$ are shown for f = 1.0, 1.2, and 1.5 in the case of an oriented system at 295 K. These results reflect the rescaling of the magnitude of electric field $F_{\rm ext}$ in terms of the local field correction f.

In the calculations for randomly oriented samples, we have fixed the ET rate constant for $P^+BH^- \rightarrow P^+BHQ^-$ as $k_{34} =$ (200 ps)⁻¹. The field-induced change in the associated free energy gap, ΔG_{34} , due to the difference in dipole moment vectors of both the ion pair states, however, should modify the value of k_{34} . The influence of the inclusion of this field dependence, $k_{34}(F_{\text{ext}})$, on the calculated results for the chargeseparation quantum yield Y_Q is examined next, using the full kinetic model. The case of an oriented system at T = 295 K is examined first, using a model for $k_{34}(F_{\text{ext}})$ given in section 2 and shown in Figure 3b. A comparison is made in Figure 13 for the charge-separation quantum yield $Y_{\rm O}(F_{\rm ext})$, in which the calculated results for the cases of fixed ($=(200 \text{ ps})^{-1}$) and fielddependent k_{34} are depicted. In the region of $F_{\text{ext}} < 0$, k_{34} decreases due to the electric field as seen in Figure 3b, thus reducing the values of $Y_Q(F_{\text{ext}})$ relative to the case of fixed k_{34} (cf. eq 2.8). The difference between both the results in Figure 13, which include the effect of static heterogeneity, is slightly smaller but comparable with the difference in Figure 2a. We also find that the effect of the field-induced variation of k_{34} on Y_0 is less than that of ΔG_{12} , ΔG_{23} , and ΔG_{13} , since the electric field dependence of k_{34} is weaker than that of $\exp(\beta \Delta G_{ii})$. Further, for the case of a randomly oriented system at T = 80

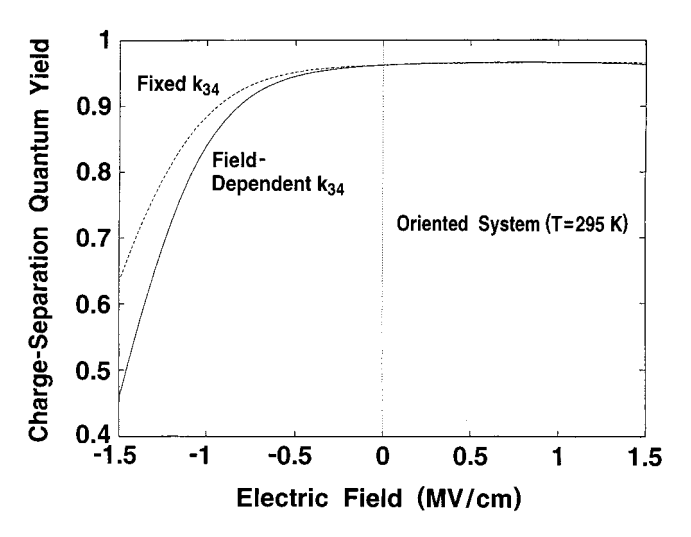


Figure 13. Effect of the inclusion of an electric field dependence of k_{34} on the behavior of $Y_Q(F_{ext})$ in the full kinetic model for an oriented system at 295 K. Dashed curve: results obtained by fixing $k_{34} = (200 \text{ ps})^{-1}$. Solid curve: results obtained with a field-dependent $k_{34}(F_{ext})$ shown in Figure 3b. The remaining conditions are the same as those in Figure 5.

K, it is seen in Figure 14 how the calculated relative values of $Y_Q(F_{\text{ext}})$ at $F_{\text{ext}} = 1.5 \text{ MV/cm}$ vary when k_{34} at this F_{ext} is varied over a considerable range of $(1000 \text{ ps})^{-1} \le k_{34} \le (50 \text{ ps})^{-1},^{58}$ using $k_{34} = (200 \text{ ps})^{-1}$ as a standard.

Appendix C: Possible Models for Modifying the Fluorescence Quantum Yield

In the calculation in section 3.3.2, k_r and k_{nr} were assumed to be independent of the electric field. The possibility that k_{nr} may be field-dependent was noted in ref 25. We remark that k_{nr} provides a decay channel which dominates k_r and that $Y_f(0)$ has an extremely small value ($\sim 4 \times 10^{-4}$ at room temperature⁵²). To make some estimate for the effect of the electric field dependence of k_{nr} due to a change in the free energy gap on the modification of the relative fluorescence quantum yield, $Y_f(F_{ext})/Y_f(0)$, in the case of a randomly oriented system at 80 K, we assume the energy gap law:⁵⁹

$$k_{\rm nr} = A \exp\left(-C \frac{|\Delta G_{10}|}{\hbar \omega}\right)$$
 (C.1)

for the nonradiative rate, noting that the free energy gap $|\Delta G_{10}|$ between the 1P*BH and PBH states has a large value. 25 In eq C.1, A and C may be regarded as constants which are nearly independent of electric field; explicitly, 59

$$C = \ln \left\{ \frac{\Delta G_{10}}{e\lambda} \left[1 - \exp \left(-\frac{\hbar \omega}{k_{\rm B} T} \right) \right] \right\}$$
 (C.2)

takes a value of the order of unity. Here, ω and λ refer to the characteristic frequency and the reorganization energy associated with the internal conversion process. Recalling that the excited and ground states have a (small) dipole moment difference of $\Delta\mu \equiv |\mu(^1\text{P*BH}) - \mu \text{ (PBH)}| \approx 6 \text{ D/f},^{27,43,45,60}$ the free energy gap ΔG_{10} is modified by the external electric field \mathbf{F}_{ext} by an amount.

$$|\Delta G_{10}(\mathbf{F}_{\text{ext}})| = \overline{\Delta G_{10}} - [\boldsymbol{\mu}(^{1}P*BH) - \boldsymbol{\mu}(PBH)] \cdot \mathbf{F}_{\text{int}}, \quad (C.3)$$

where ΔG_{10} (=11200 cm⁻¹ ²⁵) is the free energy gap at $F_{\rm ext}$ = 0 and $\mathbf{F}_{\rm int} = f\mathbf{F}_{\rm ext}$ is the induced electric field. The (angle-averaged) field-induced enhancement of $k_{\rm nr}$ in the randomly oriented sample is then estimated to be

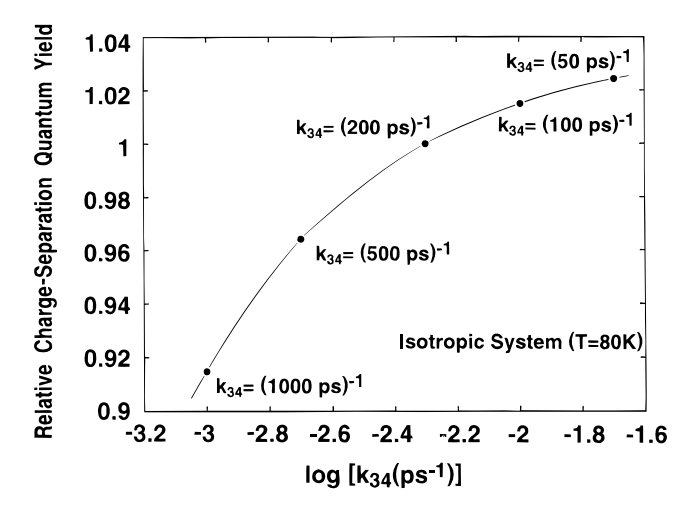


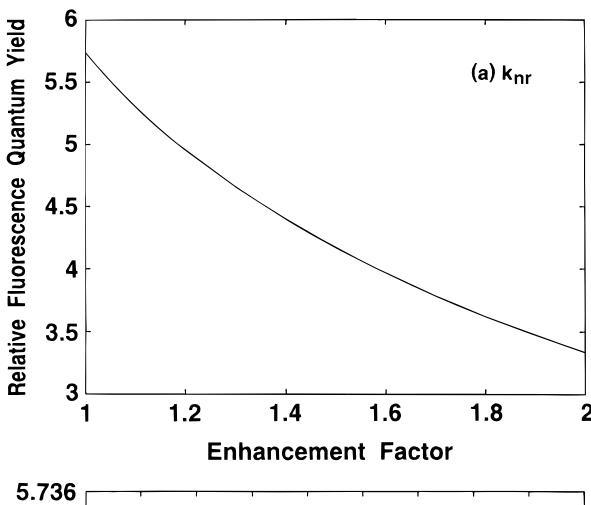
Figure 14. Dependence of the charge-separation quantum yield on the values of k_{34} in the full (quantum) kinetic model for a randomly oriented system at T=80 K and $F_{\rm ext}=1.5$ MV/cm. The calculated values of $Y_{\rm Q}$ are plotted relative to the case of $k_{34}=(200~{\rm ps})^{-1}$. The remaining conditions are the same as those in Figure 7.

$$\frac{\langle k_{\rm nr}(F_{\rm ext})\rangle}{k_{\rm nr}(0)} = \frac{1}{2} \int_{-1}^{1} d(\cos\theta) \exp\left(\frac{C\Delta\mu f F_{\rm ext}}{\hbar\omega}\cos\theta\right) = \frac{1}{\xi} \sinh\xi, \quad (C.4)$$

where $\xi \equiv C\Delta\mu f F_{\rm ext}/\hbar\omega$, $F_{\rm ext} = |{\bf F}_{\rm ext}|$, and θ is the angle between $\mu(^1{\rm P*BH}) - \mu({\rm PBH})$ and ${\bf F}_{\rm ext}$. Equation C.4 implies that $\langle k_{\rm nr}(F_{\rm ext})\rangle/k_{\rm nr}(0) > 1$ for $\xi > 0$. Quantitatively, we find that $\Delta\mu f F_{\rm ext} = 100~{\rm cm}^{-1}$ for $\Delta\mu f = 6~{\rm D}$ and $F_{\rm ext} = 1.0~{\rm MV/cm}$. The enhancement rate $\langle k_{\rm nr}(F_{\rm ext})\rangle/k_{\rm nr}(0)$ is thus estimated to be between a factor of 1 and 2 for $F_{\rm ext} = 1.0~{\rm MV/cm}$ and $T = 80~{\rm K}$, considering the uncertainty in ω and $\lambda.^{61}$ In Figure 15a the variation of $Y_{\rm f}(F_{\rm ext})/Y_{\rm f}(0)$ at $F_{\rm ext} = 1.0~{\rm MV/cm}$ is shown as a function of the enhancement factor $\langle k_{\rm nr}(F_{\rm ext})\rangle/k_{\rm nr}(0)$ for the randomly oriented system at $T = 80~{\rm K}$, based on the full (quantum) kinetic model and where $k_{\rm r}$ is fixed at $(10~{\rm ns})^{-1}.^{27,41,42,52}$ Thus, if we incorporate the field-induced enhancement of $k_{\rm nr}$ into the calculations, the agreement between calculation and experiment for $Y_{\rm f}(F_{\rm ext})/Y_{\rm f}(0)$ is improved slightly.

In addition, some dependence of k_r , k_{20} , and k_{30} on $F_{\rm ext}$ and other "hidden" pathway rates^{24,25,31} may also be responsible for the disagreement. As an example, let us consider the effect of the field-induced enhancement of k_{20} for the charge recombination process, $P^+B^-H \rightarrow PBH$. We describe the electric field dependence of k_{20} in terms of the two-mode quantum-mechanical expression, eq 2.17, in which $\lambda_{\rm m}=800~{\rm cm}^{-1},~\omega_{\rm m}=95$ cm⁻¹, $\omega_c = 1500$ cm⁻¹, and $S_c = 0.5$ are employed; the associated free energy gap is chosen as $\Delta G_{20} = -10750 \text{ cm}^{-1}$ (Table 1) without inclusion of the heterogeneity. In the case of a randomly oriented system at T = 80 K and $F_{\rm ext} = 1.0$ MV/cm, we find $\langle k_{20}(F_{\text{ext}})\rangle/k_{20}(0) = 6.2$ with the use of $|\mu(P^+B^-H)| = 51 D$ and f = 1.2. In Figure 15b the variation of $Y_f(F_{ext})/Y_f(0)$ (= $Y_d(F_{ext})/Y_d(0)$) at $F_{ext} = 1.0$ MV/cm is illustrated as a function of the enhancement factor $\langle k_{20}(F_{\text{ext}}) \rangle$ $k_{20}(0)$ on the basis of the full (quantum) kinetic model. Clearly, this calculated effect does not play a significant role for the improvement in the agreement with the experimental results in $Y_{\rm f}(F_{\rm ext})/Y_{\rm f}(0)$.

There are various uncertainties in the model parameters, as discussed in appendix B. For example, if the value of the local field correction were f=1.0 instead of f=1.2, we would find $Y_{\rm f}(F_{\rm ext})/Y_{\rm f}(0)=Y_{\rm d}(F_{\rm ext})/Y_{\rm d}(0)=4.6$ instead of 5.7 at $F_{\rm ext}=1.0$ MV/cm (then $Y_{\rm Q}(F_{\rm ext})/Y_{\rm Q}(0)=0.86$ instead of 0.81), leading to a minor improvement. However, the present model still



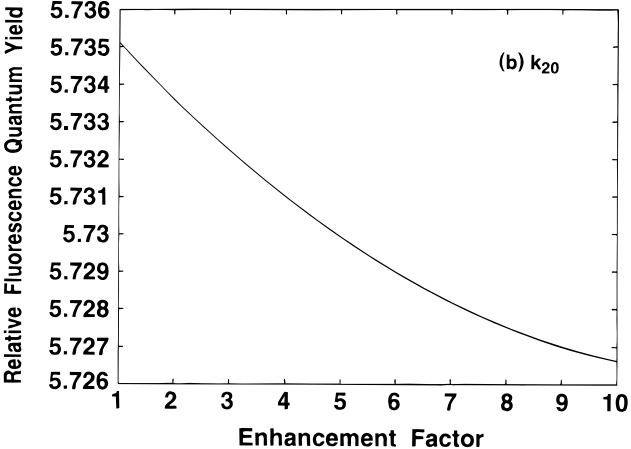


Figure 15. Relative fluorescence quantum yield, $Y_f(F_{\rm ext})/Y_f(0)$, as a function of the field-induced enhancement factor for (a) $k_{\rm nr}$ and (b) $k_{\rm 20}$ in the full (quantum) kinetic model for a randomly oriented system at T=80 K and $F_{\rm ext}=1.0$ MV/cm. In panel (a) $k_{\rm r}=(10~{\rm ns})^{-1}$ has been used. The remaining conditions are the same as those in Figure 9.

cannot reproduce the experimental results for $Y_{\rm f}(F_{\rm ext})/Y_{\rm f}(0)$ ($\sim 3-5$ in the calculation versus $\sim 1.3-2.2$ in the experiments^{27,28,30,31} at $F_{\rm ext}=1.0$ MV/cm and T=80 K), even if all the above effects are included.

Appendix D: Estimate of the Adiabaticity Parameter

We consider an expression for the ET rate constant in the classical limit ($\hbar\omega \ll k_{\rm B}T$):⁴⁶

$$k = \eta \frac{\omega}{2\pi} \exp\left[-\frac{(\lambda + \Delta G)^2}{4\lambda k_{\rm B} T}\right]. \tag{D.1}$$

Here, ω and λ refer to the characteristic frequency and reorganization energy of the vibrational modes associated with the ET reaction. The transmission coefficient may then be expressed approximately as⁶²

$$\eta \approx \begin{cases} 2\frac{1-\exp(-\gamma)}{2-\exp(-\gamma)}, & \text{for the normal region ,} \\ 2\exp(-\gamma)[1-\exp(-\gamma)], & \text{for the inverted region } \\ & (-\Delta G < \lambda), \end{cases}$$
 (D.2)

where

$$\gamma \equiv \frac{\pi V^2}{\hbar \omega} \left(\frac{\pi}{\lambda k_{\rm B} T} \right)^{1/2} \tag{D.3}$$

is an adiabaticity parameter. Equation D.2 provides an extension of the Landau–Zener formula. 46,63

For $\gamma \ll 1$, eq D.2 reduces to

$$\eta \approx 2\gamma$$
 (D.4)

in both the normal and inverted regions, thus giving the usual nonadiabatic expression:⁴⁶

$$\eta \frac{\omega}{2\pi} \approx \frac{2\pi}{\hbar} V^2 \left(\frac{1}{4\pi\lambda k_{\rm B}T}\right)^{1/2}$$
 (D.5)

The electronic coupling constant V in eqs D.3 and D.5 is a "bare" quantity. On the other hand, the coupling constant V used in the present model calculations ($V_{12} = 32 \text{ cm}^{-1}$ and $V_{23} = 59 \text{ cm}^{-1}$) in the main text should be regarded as a "renormalized" quantity which effectively takes account of the higher-order contributions through the enforced fitting to experimental ET rate within the nonadiabatic expression.

If the transmission coefficient for the P⁺B⁻H \rightarrow P⁺BH⁻ reaction is roughly estimated by the ratio of k to $\omega/2\pi$, one finds $\eta=0.39$ in the case of no electric field, upon using $k_{23}=(0.9~{\rm ps})^{-1}$ and $\omega_{\rm m}=95~{\rm cm}^{-1}$. The adiabaticity parameter then takes values of $\gamma\approx0.28$ in the normal region and $\gamma\approx0.31$ in the inverted region using eq D.2, where the latter may be more appropriate in this case because $\Delta G_{23}=-1550~{\rm cm}^{-1}$ and $\lambda_{\rm m}=800~{\rm cm}^{-1}$. The estimated adiabaticity parameter for the primary ET reactions in photosynthetic RCs is thus sizable ^{19,64,65} but still substantially less than unity. We also note that the results for the charge-separation quantum yield in the present model calculations do not depend essentially on the values of the primary ET rate constants themselves, k_{12} and k_{23} , as discussed in section 2.2 and appendix A.

References and Notes

- (1) Haberkorn, R.; Michel-Beyerle, M. E.; Marcus, R. A. *Proc. Natl. Acad. Sci. U.S.A.* **1979**, *76*, 4185.
- (2) Deisenhofer, J.; Epp, O.; Miki, K.; Huber, R.; Michel, H. J. Mol. Biol. 1984, 180, 385.
- (3) Deisenhofer, J.; Epp, O.; Miki, K.; Huber, R.; Michel, H. *Nature* **1985**, *318*, 618.
 - (4) Michel, H.; Epp, O.; Deisenhofer, J. EMBO J. 1986, 5, 2445.
- (5) Chang, C.-H.; Tiede, D.; Tang, J.; Smith, U.; Norris, J.; Schiffer, M. FEBS Lett. 1986, 205, 82.
- (6) Allen, J. P.; Feher, G.; Yeates, T. O.; Komiya, H.; Rees, D. C. Proc. Natl. Acad. Sci. U.S.A. 1987, 84, 5730.
- (7) Ermler, U.; Fritzsch, G.; Buchanan, S. K.; Michel, H. *Structure* **1994**, 2, 925.
- (8) Woodbury, N. W.; Becker, M.; Middendorf, D.; Parson, W. W. *Biochemistry* **1985**, *24*, 7516.
- (9) Martin, J.-L.; Breton, J.; Hoff, A. J.; Migus, A.; Antonetti, A. *Proc. Natl. Acad. Sci. U.S.A.* **1986**, 83, 957.
- (10) Breton, J.; Martin, J.-L.; Migus, A.; Antonetti, A.; Orszag, A. *Proc. Natl. Acad. Sci. U.S.A.* **1986**, 83, 5121.
- (11) Fleming, G. R.; Martin, J. L.; Breton, J. Nature 1988, 333, 190.
- (12) Kirmaier, C.; Holten, D. Proc. Natl. Acad. Sci. U.S.A. 1990, 87, 3552.
- (13) Holzapfel, W.; Finkele, U.; Kaiser, W.; Oesterhelt, D.; Scheer, H.; Stilz, H. U.; Zinth, W. *Proc. Natl. Acad. Sci. U.S.A.* **1990**, *87*, 5168.
- (14) Vos, M. H.; Lambry, J.-C.; Robles, S. J.; Youvan, D. C.; Breton, J.; Martin, J.-L. *Proc. Natl. Acad. Sci. U.S.A.* **1991**, 88, 8885.
- (15) Du, M.; Rosenthal, S. J.; Xie, X.; DiMagno, T. J.; Schmidt, M.; Hanson, D. K.; Schiffer, M.; Norris, J. R.; Fleming, G. R. *Proc. Natl. Acad. Sci. U.S.A.* **1992**, *89*, 8517.
- (16) Nagarajan, V.; Parson, W. W.; Davis, D.; Schenck, C. C. *Biochemistry* **1993**, *32*, 12324.
- (17) Schmidt, S.; Arlt, T.; Hamm, P.; Huber, H.; Nägele, T.; Wachtveitl, J.; Meyer, M.; Scheer, H.; Zinth, W. *Chem. Phys. Lett.* **1994**, 223, 116.
 - (18) Marcus, R. A. Chem. Phys. Lett. 1987, 133, 471.
 - (19) Marcus, R. A. Chem. Phys. Lett. 1988, 146, 13.
- (20) Michel-Beyerle, M. E.; Plato, M.; Deisenhofer, J.; Michel, H.; Bixon, M.; Jortner, J. *Biochim. Biophys. Acta* **1988**, *932*, 52.
- (21) Bixon, M.; Jortner, J.; Michel-Beyerle, M. E. Chem. Phys. 1995, 197, 389.
- (22) Popovic, Z. D.; Kovacs, G. J.; Vincett, P. S.; Alegria, G.; Dutton, P. L. *Biochim. Biophys. Acta* **1986**, *851*, 38.
- (23) Moser, C. C.; Sension, R. J.; Szarka, A. Z.; Repinec, S. T.; Hochstrasser, R. M.; Dutton, P. L. Chem. Phys. 1995, 197, 343.

- (24) Ogrodnik, A.; Langenbacher, T.; Bieser, G.; Siegl, J.; Eberl, U.; Volk, M., Michel-Beyerle, M. E. Chem. Phys. Lett. 1992, 198, 653.
- (25) Lao, K.; Franzen, S.; Stanley, R. J.; Lambright, D. G.; Boxer, S. G. J. Phys. Chem. 1993, 97, 13165.
- (26) Lao, K.; Franzen, S.; Steffen, M.; Lambright, D.; Stanley, R.; Boxer, S. G. Chem. Phys. **1995**, 197, 259.
 - (27) Lockhart, D. J.; Boxer, S. G. Chem. Phys. Lett. 1988, 144, 243.
- (28) Lockhart, D. J.; Goldstein, R. F.; Boxer, S. G. J. Chem. Phys. 1988, 89, 1408.
- (29) Lockhart, D. J.; Kirmaier, C.; Holten, D.; Boxer, S. G. J. Phys. Chem. 1990, 94, 6987.
- (30) Ogrodník, A.; Eberl, U.; Heckmann, R.; Kappl, M.; Feick, R.; Michel-Beyerle, M. E. *J. Phys. Chem.* **1991**, *95*, 2036.
 - (31) Ogrodnik, A. Mol. Cryst. Liq. Cryst. 1993, 230, 35.
- (32) Franzen, S.; Goldstein, R. F.; Boxer, S. G. J. Phys. Chem. 1990, 94, 5135.
 - (33) Franzen, S.; Boxer, S. G. J. Phys. Chem. 1993, 97, 6304.
 - (34) Bixon, M.; Jortner, J. J. Phys. Chem. 1988, 92, 7148.
- (35) Ogrodnik, A.; Keupp, W.; Volk, M.; Aumeier, G.; Michel-Beyerle, M. E. J. Phys. Chem. 1994, 98, 3432.
- (36) Sumi, H.; Kakitani, T. Chem. Phys. Lett. 1996, 252, 85; also unpublished work.
- (37) Breton, J.; Martin, J.-L.; Lambry, J.-C.; Robles, S. J.; Youvan, D. C. In *Reaction Centers of Photosynthetic Bacteria*; Michel-Beyerle, M. E., Ed.; Springer: Berlin, 1990; p 293.
- (38) Eberl, U.; Gilbert, M.; Keupp, W.; Langenbacher, T.; Siegl, J.; Sinning, I.; Ogrodnik, A.; Robles, S. J.; Breton, J.; Youvan, D. C.; Michel-Beyerle, M. E. In *The Photosynthetic Bacterial Reaction Center*; Breton, J., Verméglio, A., Eds.; Plenum Press: New York, 1992; Vol. II, p 253. (39) Ogrodnik, A. *Biochim. Biophys. Acta* 1990, 1020, 65.
- (40) Goldstein, R. A.; Takiff, L.; Boxer, S. G. *Biochim. Biophys. Acta* **1988**, *934*, 253.
- (41) Woodbury, N. W.; Parson, W. W. Biochim. Biophys. Acta 1984, 767, 345.
 - (42) Gunner, M. R.; Dutton, P. L. J. Am. Chem. Soc. 1989, 111, 3400.
 - (43) Scherer, P. O. J.; Fischer, S. F. Chem. Phys. Lett. **1986**, 131, 153.
- (44) Boxer, S. G.; Goldstein, R. A.; Lockhart, D. J.; Middendorf, T. R.; Takiff, L. J. Phys. Chem. **1989**, *93*, 8280.
- (45) Middendorf, T. R.; Mazzola, L. T.; Lao, K.; Steffen, M. A.; Boxer, S. G. *Biochim. Biophys. Acta* **1993**, *1143*, 223.
 - (46) Marcus, R. A.; Sutin, N. Biochim. Biophys. Acta 1985, 811, 265.
 - (47) Jortner, J. J. Chem. Phys. 1976, 64, 4860.
- (48) Bixon, M.; Jortner, J.; Michel-Beyerle, M. E. In *The Photosynthetic Bacterial Reaction Center*; Breton, J., Verméglio, A., Eds.; Plenum Press: New York, 1992; Vol. II, p 291; fit the data using, among other sets, $\bar{V}_{12} = 20 \text{ cm}^{-1}$ and $\bar{V}_{23} = 40 \text{ cm}^{-1}$. A later paper (ref 21) has the values of $V_{12} = 20 \text{ cm}^{-1}$ and $V_{23} = 40 \text{ cm}^{-1}$. While the latter values were labled as bare V_{ij} 's, they appear to be effective ones (\bar{V}_{ij} 's) and are related to the relevant bare ones by $\bar{V}_{ij} = V_{ij} \exp(-S_c/2)$ with $S_c = 0.5$. Thereby, they correspond to $V_{12} = 26 \text{ cm}^{-1}$ and $V_{23} = 51 \text{ cm}^{-1}$.
- (49) The minor variations in the values of V_{12} and V_{23} do not affect significantly the calculated results for the charge-separation quantum yield Y_Q . The latter is essentially determined by the detailed balance relation, eq 2.18, between the forward and backward ET rates, which is independent of the values of V_{ij} (cf. section 2.2 and appendix A).
- (50) In ref 19 it was suggested that a favorable electric field could enhance the possibility of observing the P⁺B⁻H state. In Figure 4 it is seen that this enhancement occurs not because of an increased concentration of P⁺B⁻H but rather because the P⁺B⁻H survives for a much longer time in the presence of the favorable electric field there.
 - (51) Song, X.; Marcus, R. A. J. Chem. Phys. 1993, 99, 7768.
- (52) Zankel, K. L.; Reed, D. W.; Clayton, R. K. *Proc. Natl. Acad. Sci. U.S.A.* **1968**, *61*, 1243.
- (53) The experimental data in the literature are scattered substantially. References 27 and 28 have observed an increase in the fluorescence quantum yield by 25% at $F_{\rm ext}=0.89$ MV/cm. Reference 30 has reported the increase by 40% at $F_{\rm ext}=0.7$ MV/cm. If we assume a quadratic electric field dependence of the increment of the fluorescence quantum yield observed experimentally, $^{28.30}$ we will find enhancement factors of 1.3 and 1.8, respectively, at $F_{\rm ext}=1.0$ MV/cm. In addition, larger values for the enhancement factor, 1.6 and 1.9, are found in ref 31 for $F_{\rm ext}=0.7$ and 1.0 MV/cm, respectively.
- (54) Osváth, S.; Laczkó, G.; Sebban, P.; Maróti, P. Photosynth. Res. 1996, 47, 41.
- (55) The good agreement of the calculated results between the simplified model and the full kinetic model, shown in the following, does not depend on this choice for the value of α . As will be shown in Figure 11, eq 2.8 reproduces the numerical results well also in the absence of any heterogeneity
- (56) In Figure 10, the value of Y_Q increases with the increase in the free energy gap, $|\Delta G_{23}(F_{\rm ext}=0)|$, in spite of the pertinent ET reaction being in the inverted region (cf. section 3.1). This behavior, which perhaps is at first glance surprising, is due to the fact that the charge-separation quantum yield primarily depends not on the forward ET rate constant but on the detailed balance relation, eq 2.18, between the forward and backward ET rates, as suggested by eqs 2.6–2.8.

- (57) The value of the free energy gap, ΔG_{12} , may contain a considerable experimental uncertainty, resulting in a large margin of error in the calculated value of the charge-separation quantum yield Y_Q . However, the error in Y_Q arising from the uncertainty in ΔG_{12} is supposed to be relatively small, because the value of $Y_{\rm Q}$ is predominantly governed by more reliable quantities, ΔG_{23} and $\Delta G_{13} = \Delta G_{12} + \Delta G_{23}$, as seen in eqs 2.6–2.8. (58) There are two possibilities which may modify the value of k_{34} from (200 ps)⁻¹ in the case of randomly oriented samples at T=80 K. First,
- the applied electric field would tend to reduce k_{34} irrespective of the relative orientation to the dipole moment vectors of the ion pair states, as seen in Figure 3b. Second, the lowering of the temperature would enhance k_{34} , although this effect is known to be minor.42
- (59) Englman, R.; Jortner, J. Mol. Phys. 1970, 18, 145.
- (60) Lockhart, D. J.; Hammes, S. L.; Franzen, S.; Boxer, S. G. J. Phys. Chem. 1991, 95, 2217.
- (61) If we employ $\omega = 95 \text{ cm}^{-1}$ and $\lambda = 800 \text{ cm}^{-1}$ for the low-frequency medium vibrational modes, we find $\xi = 1.53$ and $\langle k_{\rm nr}(F_{\rm ext}) \rangle / k_{\rm nr}(0) = 1.44$. On the other hand, if we use $\omega = 1500~{\rm cm}^{-1}$ and $\lambda = 750~{\rm cm}^{-1}$ for the high-frequency intramolecular vibrational modes, we find $\xi=0.11$ and $\langle k_{\rm nr}(F_{\rm ext}) \rangle / k_{\rm nr}(0) = 1.002.$
 - (62) Sumi, H. J. Phys. Soc. Jpn. **1980**, 49, 1701.
 - (63) Newton, M. D. Chem. Rev. 1991, 91, 767.
 - (64) Marcus, R. A.; Almeida, R. J. Phys. Chem. 1990, 94, 2973.(65) Almeida, R.; Marcus, R. A. J. Phys. Chem. 1990, 94, 2978.